Viscous irrotational theories and the force on an expanding bubble–A cell-model analysis*

Juan C. Padrino
University of Minnesota, Department of Aerospace Engineering and Mechanics, Minneapolis, MN 55455, USA

Daniel D. Joseph†
University of Minnesota, Department of Aerospace Engineering and Mechanics, Minneapolis, MN 55455, USA
University of California, Irvine, Department of Mechanical & Aerospace Engineering, Irvine, CA 92697, USA

Abstract

The dynamics of a bounded viscous incompressible fluid surrounding a spherical bubble in rectilinear motion simultaneously experiencing volume changes is examined by means of two viscous irrotational theories, namely, viscous potential flow and the dissipation method. The forces that the liquid produces on the bubble and on the outer spherical boundary of the liquid are determined from these two approaches at the instant when the bubble is concentric with the outer surface. Viscous potential flow involves surface integration of the irrotational normal stress; the dissipation method stems from the mechanical energy balance, including the dissipation integral, evaluated in potential flow. In the inner boundary, zero tangential stress is enforced. Two choices for the tangential stress condition on the outer boundary are considered: Zero tangential stress or irrotational tangential stress. In a sense, this is an extension to include viscous effects of the inviscid analysis by Sherwood [*Int. J. Multiphase Flow*, **25**, 705, 1999]. The potential flow that follows from Sherwood's work is used in the derived formulae to compute the drag. To the added-mass forces associated with the bubble acceleration and rate of change of the bubble radius determined by Sherwood, a viscous contribution is added here that depends upon the instantaneous bubble velocity and the inner and outer instantaneous radii of the bubble-liquid cell. When the outer radius is taken to infinity, the expressions for the drag yield results given in the literature. If the inner and outer radii are held fixed, results from the cell model may be used to approximate the drag on a bubble moving in a bubbly flow with the same volume fraction as the cell. The analysis yields two results for the viscous drag on the bubble contingent on the boundary condition applied on the outer sphere. These formulas have been presented in the literature, although regarded as contradictories. By emphasizing the role of the tangential stress on the outer boundary, it is shown that both results are valid as they depend on the choice of the outer dynamic boundary condition. These results agree to first order in the volume fraction. The terminal rise velocity of a bubble swarm is derived using the drag from the viscous irrotational theories. Results for the drag coefficient and bubble rise velocity are compared with other theoretical results as well as data from numerical simulations and experiments.

1 Introduction

Bubbly flows in the regime of high Reynolds and low Weber numbers exhibit bubbles that are spherical or nearly spherical. Here these groups are defined in the usual way; the former $Re \equiv 2Ua/\nu$ and the latter $We \equiv 2\rho U^2 a/\sigma$, U being the bubble relative velocity, a the bubble radius, ρ and ν the density and kinematic viscosity of the liquid, respectively, and σ the interfacial tension. In general, for very high Reynolds numbers ($O(1000)$, say[1]), the Weber number is likely greater than unity and the bubble shows

*With an appendix by R. Fosdick and J. C. Padrino.

†To whom correspondence should be addressed. Phone: +1-612-625-0309. Fax: +1-612-626-1558. E-mail: joseph@aem.umn.edu

important deviations from the spherical shape. Experimentally, the dual limit of high Reynolds and low Weber numbers have been realized with $Re = O(100)$ and $We = O(1)$, respectively[2]. For instance, bubbles with a diameter in the order of 1 mm rising in water satisfy the dual condition of high Reynolds and low Weber numbers[2,3]. Moreover, in this regime, with a clean liquid, that is, free of impurities and surfactants, vorticity effects are confined to a thin boundary layer on the bubble surface and to a wake in a minute neighborhood of the bubble rear end[1]. Therefore, liquid motion in the bulk can be considered irrotational. Because of these features, bubbly flows in this regime are particularly suited for analysis. Further simplification is attained by considering bubbles of the same diameter, that is, a monodispersed suspension. In practice, small variation about the mean bubble diameter may be achieved by preventing coalescence with the addition of certain chemicals to the mixture in such low concentration that the gas-liquid interface does not behave as the boundary of a rigid particle, in which case a recirculation zone would appear at the rear side of the bubble, thereby breaking down the irrotational hypothesis[2,4].

For bubbles rising under the action of gravity, the problem have also been described, besides the Reynolds number, by the Eötvös number, which is a characteristic of the bubble size, and the Morton number, which is a group that involves physical properties with no bubble size-dependent quantities[5]. Small Eötvös numbers are associated with nearly spherical bubbles, whereas larger Eötvös indicates highly distorted bubbles. The Weber number can be recovered by combining those three dimensionless groups. Instead of the Morton number, the Archimedes number may be used[6].

In modeling bubbly flows in the regime of low Weber and high Reynolds numbers, viscous drag is usually computed from the liquid potential flow solution exploiting the fact that rotational (viscous) deviations from irrotational motion are confined to thin regions adjacent to the bubbles. In this regard, the dissipation method, based upon the mechanical energy balance, has been a commonly used approach. A boundary layer on a clean bubble interface conforms to the zero-shear-stress boundary condition, because of the large viscosity of the liquid compared to the small viscosity of the gas, rather than to the no-slip constraint enforced on a solid particle. This boundary layer remains attached almost over the entire bubble interface, as separation occurs only around the rear end. Since vorticity is contained in these narrow regions, it is assumed that the rate of viscous dissipation is given entirely by the irrotational motion[7].

For a sphere translating in rectilinear motion with constant speed within an infinite liquid, the dissipation approximation seems to have been applied first by Bateman in 1931 (see Dryden, Murnaghan and Bateman[8], p. 157) who obtained the drag $12\pi a\mu U$, where μ is the liquid dynamic viscosity. Later, Ackeret[9] repeated this dissipation calculation. For a bubble in rectilinear motion, Levich (1949)[10] applied the dissipation method and attained the result given above. This drag is close to the measured value for Reynolds numbers above 20, say[11]. It should be noted that for a ridig sphere, with the no-slip condition enforced at its surface, or a spherical bubble of constant volume, for which the tangential component of the traction vanishes at the interface, the dissipation calculation based on potential flow gives rise to the same drag[11]. Moore[12] found the drag $12\pi a\mu U$, which in dimensionless form is written as $48/Re$, by computing the momentum deficit. In addition, he determined the structure of the boundary-layer flow and used this information to improve upon the Re^{-1} result by adding a $Re^{-3/2}$ contribution from the dissipation in the boundary layer and wake. Kang and Leal[13] and, recently, Joseph and Wang[14] used different methods to add a viscous correction to the normal stress and obtained $48/Re$. It should be noted that Moore[15] computed a viscous drag by direct integration of the irrotational normal stress around the bubble, thereby enforcing the zero shear stress at the interface. He found the drag $8\pi a\mu U$, which fell short of the dissipation result. Evidently, this discrepancy is resolved by adding a viscous correction to the irrotational normal stress[12–14]. Tam[16] extended Moore's[12] analysis to the case of a translating bubble undergoing acceleration and found the same form of the viscous drag. The approach of potential flow with viscous normal stresses at a gas-liquid interface was employed by Miksis, Vanden-Broeck and Keller[17] to compute numerically the shape of a rising bubble using a boundary-integral formulation.

The effect of a varying bubble radius on the force experienced by a bubble translating in an un-

bounded liquid has been the subject of a number of works. Magnaudet and Legendre[18] examined this case by means of a frame transformation under which the bubble radius becomes fixed while conserving dynamic similarity. The total force on the bubble is presented for both the inertia-dominated flow and the creeping flow limits. Ohl, Tijink and Prosperetti[19] conducted experimental investigations of this bubble motion, whereas Yang, Prosperetti and Takagi[20] carried out numerical simulations. Both works included simplified dynamic models accounting for the forces acting on a bubble that compare favorably with the experimental and numerical data. Takemura and Magnaudet[21] studied experimentally the history force on a shrinking bubble rising at finite Reynolds number. Recently, Léger and Askovic[22] carried out the modeling of the boundary layers outside and within a slowly deforming spherical bubble in rectilinear motion. Comprehensive reviews on the advances in the understanding of single bubble dynamics have been given by Magnaudet and Eames[23] and Kulkarni and Joshi[24].

Dynamic simulations of the motion of a set of N bubbles moving in a liquid at rest at infinity have been examined in several papers (Voinov and Golovin[25]; Gavrilyuk and Teshukov[26]; Ilinsky, Hamilton and Zabolotskaya[27]). Smereka[28] studied the motion of a set of bubbles in a box in a periodic assembly, so that the entire space is filled with an array of boxes. Wang and Smereka[29] took the continuum limit of the equations of motion for a finite set of bubbles in an unbounded liquid to obtain effective equations in terms of the void fraction. In these works, potential flow is assumed for the liquid motion and viscous effects are given by the dissipation method. Sangani and Didwania[3] and Kushch *et al.*[30] performed dynamic simulations with the viscous drag determined from a leading order viscous correction to the irrotational pressure computed from the analysis of the boundary layer flow around the bubbles. The former also estimated the viscous drag on the bubbles with the gradient of the rate of energy dissipation in potential flow. The latter considered arrays of ellipsoids to account for bubble shape deformation such that flows with finite Weber numbers may be simulated. On the other hand, averaged equations for bubbly flows derived from first principles have been presented by Sangani[31] and Spelt and Sangani[32] considering the irrotational motion of a viscous fluid, and in Zhang and Prosperetti[33] for an inviscid fluid. Recently, the buoyant rise of a set of nearly spherical bubbles as well as deformable ones at $O(100)$ Reynolds number in a periodic box has been studied through direct numerical simulations of the incompressible Navier-Stokes equations by Esmaeeli and Tryggvason[6] with a front tracking/finite-volume method. Earlier, these authors[34,35] applied a similar method to study nearly spherical bubbles at $Re = O(1)$ and $Re \approx 20$. Using the same technique, Bunner and Tryggvason[36,37] considered a much larger number of bubbles for the latter Reynolds-number regime. By placing a single bubble in a periodic box, a regular array of bubbles of the same size was simulated by Sankaranarayanan *et al.*[5] and Yin *et al.*[38] using the lattice Boltzmann method for the intermediate-Reynolds-number regime, i.e. $O(10)$. In this regime, the wake effects in the bubble-liquid dynamics cannot be neglected. Careful experiments and detailed measurements have been carried out by Zenit *et al.*[2] to study bubbly flow for small Weber and large Reynolds numbers and by Martinez-Mercado *et al.*[39] for intermediate and high Reynolds numbers in the range 10 to 500.

Effective properties of particulate flows including hydrodynamic transport coefficients have been modeled by means of effective-medium theories. According to these approximate theories, the conditionally-averaged field satisfies the suspending fluid equations within a suitably sized exclusion region that encloses a reference particle or bubble and the unconditionally-averaged fields in the effective medium occupying the rest of the space[40]. The method does not bear the ambiguity of the choice of proper constraints at the interface between the effecttive medium and the exclusion region. Kushch *et al.*[30] determined the added mass and viscous drag coefficients for a suspension of oblate spheroidal bubbles using an effective medium theory showing remarkable agreement with dynamic simulations. Detailed descriptions of the effective medium theory applied in various contexts can be found elsewhere[41–44].

A simplified approach to examine the hydrodynamics of bubbly flow for small or moderate gas volume fraction is obtained through the so-called 'cell-model' representation. For nearly spherical bubbles, the bubbly flow is assumed to be composed of identical unit spherical cells. Each cell consists of a spherical bubble surrounded by a liquid bounded by an outer spherical envelope concentric with the bubble. The

outer sphere radius is such that the cell void fraction is identical to the void fraction of the bubbly flow[45]. The underlying hypothesis is that the dynamics within the reference cell is representative of the dynamics in the entire bubbly flow. The choice of the outer boundary condition in the cell model has been subject of debate (see Chhabra[46] and references therein). Happel and Brenner[45] argue that each cell should be a unit independent of the rest of the assemblage, so no energy exchange takes place with its surroundings. They thus consider that a frictionless outer boundary is adequate. Other boundary conditions, however, have been applied in the literature. For particulate flows in the limit of creeping motion, Cunningham[47] applied the cell model with no-slip conditions on the inner and outer spherical boundaries. Happel[48] considered the same problem although imposing a zero-tangential-stress constraint on the outer envelope. Kuwabara[49] applied a zero-vorticity boundary condition on the outer sphere and computed the drag from the dissipation integral evaluated in Stokes' flow. However, in his formulation, as pointed out by El-Kaissy and Homsy[50], the term accounting for the work of the tangential stress on the outer envelope is missing. The zero-vorticity constraint implies that mechanical energy is transferred between the reference cell and the rest of the domain. For higher Reynolds numbers, Marrucci[51] employed the cell model to predict the drag on the bubble evaluating the dissipation integral from the potential flow solution in the cell. Recently, Kendoush[52] revisited Marrucci's analysis obtaining a different drag. We shall review this discrepancy in §3. Leclair and Hamielec[53] presented the numerical solution of the Navier-Stokes equations for the liquid motion within a unit cell with zero shear stress on the bubble surface and zero vorticity on the outer sphere. They computed the drag on the bubble with the numerical flow field. Reasonably good agreement with experimental data was reported. A similar numerical analysis was performed by Manjunath *et al.*[54] enforcing, on the contrary, a zero-tangential-stress condition on the outer boundary. Chhabra[46] also presented numerical results for a viscous liquid in a cell model enclosing a bubble to elucidate the effect on the drag of the choice of either zero tangential stress (free surface) or zero vorticity on the outer boundary. He concluded that the viscous force shows a stronger dependence on the void fraction in the zero-vorticity model than in the free-surface model. All these works have considered a cell enclosing a bubble of constant volume. More recently, Sherwood[55] modeled the dynamics of a translating spherical bubble with a time dependent radius surrounded by an inviscid imcompressible fluid bounded externally by a spherical surface. He presented expressions for the force on the bubble and on the outer envelope.

After surveying the literature on the cell model, we are left with the impression that the implementation of the dissipation method lacks a systematic approach to deriving expressions for the forces starting from the mechanical energy equation with emphasis in the role of the cell boundary conditions from dynamics (stresses). The aim of this paper is to extend Sherwood's[55] analysis to include viscous effects by use of purely irrotational theories, namely, viscous potential flow and the dissipation approximation. The former approach computes the force on a given direction by direct integration of the irrotational normal stress over the boundary, whereas the latter predicts the drag from the mechanical energy balance evaluated in potential flow, so that the viscous effects arise from the rate of energy dissipation. First, working formulae for the drag is developed by applying these theories to the system defined by a spherical bubble with its center moving in a rectilinear path and undergoing volume changes within a bounded liquid domain with a deforming outer boundary. The shape evolution of the inner and outer boundaries is assumed to be known, such that the incompressibility constraint is satisfied. Two different conditions for the tangential stress on the outer boundary are considered, namely, a zero-tangential-stress condition (i.e. free surface) and an irrotational-tangential-stress condition. In the inner boundary (i.e. bubble surface), zero tangential stress is enforced. This is the same as having two boundary-value problems. The dissipation method gives rise to different expressions for the force on the bubble on a given direction depending upon the tangential stress condition applied on the outer boundary of the reference cell. Viscous potential flow, on the other hand, gives the same bubble drag independently of the choice of the outer boundary condition. Next, the flow field is obtained from Sherwood's potential analysis. This potential flow is then entered in the machinery derived before to compute the forces on the spherical bubble and on the spherical outer envelope at the

instant when both are concentric. This is the same geometric condition for which Sherwood computed the forces. The expressions for the drag on the bubble show the added-mass contribution given by the acceleration of the bubble translational motion and the rate of change of the bubble radius, already given in Sherwood's inviscid analysis, plus a viscous drag depending upon the instantaneous values of the velocity and inner and outer radii. When neither the inner nor the outer radius changes with time, the formulas for the drag are rewritten in terms of the cell void fraction. According to the cell model, these expressions can be used as an approximation for the drag on a typical bubble moving in a bubbly flow with the same average void fraction. These results for the viscous drag from the dissipation method have been given in the literature[51,52]; however, the role of the dynamic boundary conditions, in particular, that of the tangential stress on the outer boundary, is not evident there. Because each of these two expressions for the drag corresponds to a different choice of the outer boundary condition for the stress, these results do not contradict each other, neither is one of them in error, as has been argued in the literature[52]. Results indicate that the drag from the model with an irrotational tangential stress on the outer boundary shows a stronger dependence upon the void fraction than the drag from a free-surface cell model. Both results for the bubble drag from the dissipation method, however, match to first order in the void fraction. Using the formulae for the drag, expressions for the terminal rise velocity for a bubble swarm in dimensionless form are obtained. Finally, predictions from these analyses are compared with results from other theoretical approaches, numerical simulations and experiments.

2 Formulae for the force on an expanding bubble within a bounded liquid from viscous irrotational theories

We present the analysis that gives rise to the formulae for the force acting on a spherical compressible bubble along its direction of motion within a liquid confined by a spherical surface. Two types of purely irrotational analysis are carried out, namely, viscous potential flow and the dissipation method.

2.1 Problem formulation

Consider a spherical bubble B moving within a viscous incompressible Newtonian fluid occupying the volume V in three dimensions. Let S_1 be the interface shared by the bubble B and the liquid in V and let S_2 be the outer spherical surface bounding V (figure 1). Both, S_1 and S_2 remain spherical during the entire motion. Suppose the center of the bubble moves on a straight line containing the center of the outer sphere S_2 along the direction $\mathbf{e}_x$ (fixed) with velocity U, which may be a function of time. Moreover, suppose the bubble volume can change with time but the bubble does not rotate. The pathline followed by the center of the bubble thus defines the axis of symmetry for this configuration. Let $\mathbf{u}$ be the velocity field in the laboratory (inertial) reference frame. Let $\mathbf{v}$ be the velocity field with respect to a noninertial reference frame whose origin moves with velocity $U\mathbf{e}_x$ relative to the laboratory frame, but it is not allowed to rotate. Velocities $\mathbf{u}$ and $\mathbf{v}$ are then related by

$$\mathbf{u} = U\mathbf{e}_x + \mathbf{v}. \tag{2.1}$$

The fluid dynamics within the bubble does not enter the analysis. Suppose the following boundary conditions are given:

On S_1,

$$\mathbf{n}_1 \cdot \mathbf{v} = \hat{q}_1, \tag{2.2}$$

$$\mathbf{n}_1 \cdot \mathbf{T} \cdot \mathbf{t}_1^{(\alpha)} = 0, \qquad \text{with} \quad \mathbf{t}_1^{(\alpha)} \perp \mathbf{n}_1, \tag{2.3}$$

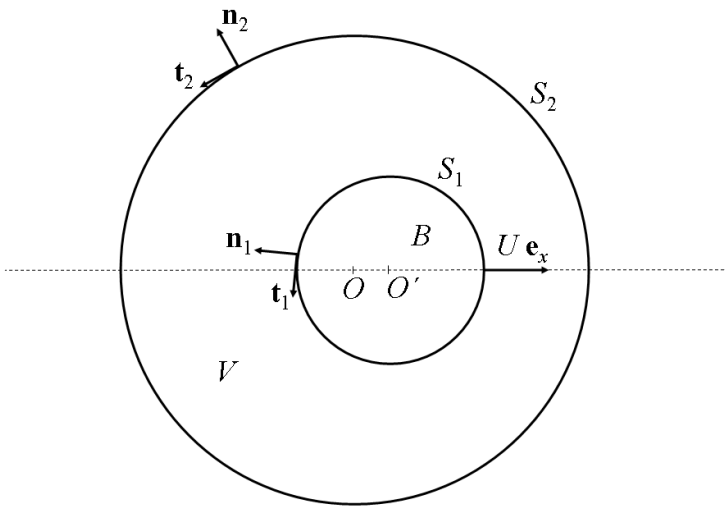

Figure 1: Sketch of a spherical bubble B centered at O' sharing interface S_1 with the incompressible fluid occupying volume V bounded externally by the spherical surface S_2 centered at O. The motion of the bubble B is such that O' moves along the fixed direction $\mathbf{e}_x$ with speed U, and its radius can change with time. The line containing the path of O' also contains O, which is fixed with respect to the laboratory frame. This line is therefore the axis of symmetry of the problem. The separation between O and O' is considered to be small. Because of the incompressibility of the fluid in V, changes in the radius of S_2 occur in accordance with changes in the radius of B. Symbol $\mathbf{n}_1$ denotes the inward unit vector to V on S_1 and $\mathbf{n}_2$ denotes the outward unit vector to V on S_2. Unit vectors $\mathbf{t}_1$ and $\mathbf{t}_2$ are orthogonal to $\mathbf{n}_1$ and $\mathbf{n}_2$, respectively.

On S_2,

$$\mathbf{n}_2 \cdot \mathbf{u} = q_2, \tag{2.4}$$

$$\mathbf{n}_2 \cdot \mathbf{T} \cdot \mathbf{t}_2^{(\alpha)} = \tau_2^{(\alpha)}, \qquad \text{with} \quad \mathbf{t}_2^{(\alpha)} \perp \mathbf{n}_2, \tag{2.5}$$

and $\alpha = 1, 2$. Here, $\mathbf{n}_1$ is the inward unit normal on S_1 to V (i.e. outward to the bubble) and $\mathbf{n}_2$ is the outward unit normal on S_2 to V; $\mathbf{t}_1^{(\alpha)}$ and $\mathbf{t}_2^{(\alpha)}$ are unit vectors. Each triad $\{\mathbf{n}_\beta, \mathbf{t}_\beta^{(1)}, \mathbf{t}_\beta^{(2)}\}$, with $\beta = 1, 2$, is orthogonal and right-handed. Symbol $\mathbf{T}$ denotes the stress tensor.

Constraint (2.3) is a standard interfacial condition for a bubble, in which case the gas dynamic viscosity is small in comparison to that of the liquid. We are assuming here that Marangoni stresses, which originate from surface tension gradients, are negligible. This is typical of a clean gas-liquid interface (e.g., free of impurities or surfactants). From (2.1) and (2.2), notice that $q_1 = \mathbf{n}_1 \cdot \mathbf{u} = U\mathbf{n}_1 \cdot \mathbf{e}_x + \hat{q}_1$ on S_1.

Two choices for $\tau_2^{(\alpha)}$ in (2.5) for the outer boundary are considered in this work, namely, (i) zero tangential stress and (ii) irrotational tangential stress. The latter is established from the potential flow in V, which is fully determined by kinematic boundary conditions as explained in §2.2.

Using (2.2) and (2.4), the incompressibility condition and divergence theorem lead to

$$\int_{S_1} \hat{q}_1 dA = \int_{S_2} q_2 dA, \tag{2.6}$$

which establishes a constraint that $\hat{q}_1$ and q_2 must satisfy.

The forces that the fluid in V exerts on S_1 and S_2 in the $\mathbf{e}_x$ direction are

$$D_1 \equiv \int_{S_1} \mathbf{n}_1 \cdot \mathbf{T} \cdot \mathbf{e}_x dA, \tag{2.7}$$

$$D_2 \equiv -\int_{S_2} \mathbf{n}_2 \cdot \mathbf{T} \cdot \mathbf{e}_x dA. \tag{2.8}$$

With the decomposition $\mathbf{e}_x = \mathbf{n}_\beta(\mathbf{n}_\beta \cdot \mathbf{e}_x) + \mathbf{t}_\beta^{(\alpha)}(\mathbf{t}_\beta^{(\alpha)} \cdot \mathbf{e}_x)$, for $\alpha = 1, 2$ and $\beta = 1, 2$, with summation over α but not over β, these expressions can be written as

$$D_1 = \int_{S_1} \mathbf{n}_1 \cdot \mathbf{T} \cdot \mathbf{n}_1(\mathbf{n}_1 \cdot \mathbf{e}_x) dA + \int_{S_1} \mathbf{n}_1 \cdot \mathbf{T} \cdot \mathbf{t}_1^{(\alpha)}(\mathbf{t}_1^{(\alpha)} \cdot \mathbf{e}_x) dA, \tag{2.9}$$

$$D_2 = -\int_{S_2} \mathbf{n}_2 \cdot \mathbf{T} \cdot \mathbf{n}_2(\mathbf{n}_2 \cdot \mathbf{e}_x) dA - \int_{S_2} \mathbf{n}_2 \cdot \mathbf{T} \cdot \mathbf{t}_2^{(\alpha)}(\mathbf{t}_2^{(\alpha)} \cdot \mathbf{e}_x) dA. \tag{2.10}$$

Invoking constraints (2.3) and (2.5), we have

$$D_1 = \int_{S_1} \mathbf{n}_1 \cdot \mathbf{T} \cdot \mathbf{n}_1(\mathbf{n}_1 \cdot \mathbf{e}_x) dA, \tag{2.11}$$

$$D_2 = -\int_{S_2} \mathbf{n}_2 \cdot \mathbf{T} \cdot \mathbf{n}_2(\mathbf{n}_2 \cdot \mathbf{e}_x) dA - \int_{S_2} \tau_2^{(\alpha)}(\mathbf{t}_2^{(\alpha)} \cdot \mathbf{e}_x) dA. \tag{2.12}$$

It is assumed in this analysis that the geometry of the fluid domain V is known at any time. For the sake of simplicity, we have taken hydrostatics forces (i.e. buoyancy) out of the analysis.

2.2 Viscous potential flow

The viscous potential flow approximation of the forces on surfaces S_1 and S_2 is obtained by direct integration of the stress computed for purely irrotational motion. For a free-shear surface, where the actual tangential stress is zero, only the normal stress enters in the viscous potential flow computation even though the irrotational tangential stress is not zero.

For irrotational motion, the velocity field is $\mathbf{u} = \nabla\phi = U\mathbf{e}_x + \mathbf{v}$. For incompressible flow, the potential satisfy

$$\nabla^2\phi = 0, \tag{2.13}$$

with boundary conditions

$$\mathbf{n}_1 \cdot \nabla\phi = q_1 = U\mathbf{n}_1 \cdot \mathbf{e}_x + \hat{q}_1 \tag{2.14}$$

on S_1, and

$$\mathbf{n}_2 \cdot \nabla\phi = q_2 \tag{2.15}$$

on S_2. The irrotational pressure p satisfies the Bernoulli equation:

$$\frac{p}{\rho} + \frac{\partial\phi}{\partial t} + \frac{|\mathbf{u}|^2}{2} = C(t). \tag{2.16}$$

The forces on the boundaries of V are computed according to (2.11) and (2.12) for irrotational motion. For a Newtonian fluid, the stress tensor is thus given by

$$\mathbf{T} = -p\mathbf{1} + 2\mu\nabla \otimes \nabla\phi. \tag{2.17}$$

Hereinafter, for the sake of brevity, we use the symbol $\mathbf{D} \equiv \nabla \otimes \nabla\phi$ to refer to the strain-rate tensor in potential flow.

On the free-shear surface S_1 or bubble interface, the force in the $\mathbf{e}_x$ direction is

$$D_1 = \int_{S_1} \left(-p + \mathbf{n}_1 \cdot 2\mu\mathbf{D} \cdot \mathbf{n}_1\right) \mathbf{n}_1 \cdot \mathbf{e}_x dA. \tag{2.18}$$

The force on the outer free surface S_2 in the $\mathbf{e}_x$ direction is, for zero tangential stress,

$$D_2 = -\int_{S_2} \left(-p + \mathbf{n}_2 \cdot 2\mu\mathbf{D} \cdot \mathbf{n}_2\right) \mathbf{n}_2 \cdot \mathbf{e}_x dA. \tag{2.19}$$

In the case of an outer boundary subject to a tangential stress given by the potential flow in the interior, that is,

$$\tau_2^{(\alpha)} = \mathbf{n}_2 \cdot 2\mu\mathbf{D} \cdot \mathbf{t}_2^{(\alpha)}, \tag{2.20}$$

the self-equilibration of irrotational viscous stresses on a closed surface (Appendix B) implies

$$\int_{S_1} \mathbf{n}_1 \cdot 2\mu\mathbf{D} \cdot \mathbf{e}_x dA = \int_{S_2} \mathbf{n}_2 \cdot 2\mu\mathbf{D} \cdot \mathbf{e}_x dA = 0. \tag{2.21}$$

Hence,

$$D_2 = -\int_{S_2} (-p)\, \mathbf{n}_2 \cdot \mathbf{e}_x dA. \tag{2.22}$$

Thus, the force on the outer boundary is obtained solely from the irrotational pressure in this case.

2.3 Dissipation method

In this section, the computation of the forces on the inner and outer boundaries of the fluid domain oriented along the direction of bubble translation are obtained by used of the dissipation approximation based upon irrotational motion. For the outer boundary, in addition to the kinematic constraint imposed on the normal velocity, two choices are considered for the shear stress, as in §2.2: (i) Zero tangential stress and (ii) irrotational tangential stress. Each of these possibilities leads to a set of results that are compared with those from viscous potential flow.

Suppose now that the fluid motion in V is governed by the incompressible Navier-Stokes equations with an appropriate set of boundary conditions that includes (2.2)-(2.5). The rate of change of kinetic energy in V is

$$\frac{dE}{dt} = \frac{d}{dt}\int_V \rho\frac{|\mathbf{u}|^2}{2}\,d\mathcal{V} = \int_V \mathbf{u}\cdot\rho\left(\frac{\partial\mathbf{u}}{\partial t} + \mathbf{u}\cdot\nabla\mathbf{u}\right)d\mathcal{V}. \tag{2.23}$$

The last equality in (2.23) follows from the fact that mass crosses neither S_1 nor S_2. The fluid has density ρ and dynamic viscosity μ. From (2.23), the Navier-Stokes equations and divergence theorem lead to

$$\frac{dE}{dt} = -\int_{S_1}\mathbf{n}_1\cdot\mathbf{T}\cdot\mathbf{u}\;dA + \int_{S_2}\mathbf{n}_2\cdot\mathbf{T}\cdot\mathbf{u}\;dA - \int_V 2\mu\mathbf{D}[\mathbf{u}]:\mathbf{D}[\mathbf{u}]\;d\mathcal{V}, \tag{2.24}$$

where $\mathbf{T}$ is the stress tensor for a Newtonian fluid and the strain-rate tensor

$$\mathbf{D}[\mathbf{u}] = \frac{1}{2}(\nabla\mathbf{u} + \nabla\mathbf{u}^T). \tag{2.25}$$

Using (2.1) and (2.7), expression (2.24) leads to

$$UD_1 = -\frac{dE}{dt} - \int_{S_1}\mathbf{n}_1\cdot\mathbf{T}\cdot\mathbf{v}\;dA + \int_{S_2}\mathbf{n}_2\cdot\mathbf{T}\cdot\mathbf{u}\;dA - \int_V 2\mu\mathbf{D}[\mathbf{u}]:\mathbf{D}[\mathbf{u}]\;d\mathcal{V}. \tag{2.26}$$

Expanding the surface integrals, this expression may be written as

$$\begin{aligned} UD_1 &= -\frac{dE}{dt} - \int_{S_1}\mathbf{n}_1\cdot\mathbf{T}\cdot\mathbf{n}_1(\mathbf{n}_1\cdot\mathbf{v})\;dA - \int_{S_1}\mathbf{n}_1\cdot\mathbf{T}\cdot\mathbf{t}_1^{(\alpha)}\left(\mathbf{t}_1^{(\alpha)}\cdot\mathbf{v}\right)\;dA \\ &+ \int_{S_2}\mathbf{n}_2\cdot\mathbf{T}\cdot\mathbf{n}_2(\mathbf{n}_2\cdot\mathbf{u})\;dA + \int_{S_2}\mathbf{n}_2\cdot\mathbf{T}\cdot\mathbf{t}_2^{(\alpha)}\left(\mathbf{t}_2^{(\alpha)}\cdot\mathbf{u}\right)\;dA \\ &- \int_V 2\mu\mathbf{D}[\mathbf{u}]:\mathbf{D}[\mathbf{u}]\;d\mathcal{V}. \end{aligned} \tag{2.27}$$

With boundary conditions (2.2)-(2.5), we have

$$D_1 = \frac{1}{U}\left(-\frac{dE}{dt} - \int_V 2\mu\mathbf{D}[\mathbf{u}]:\mathbf{D}[\mathbf{u}]\;d\mathcal{V} + W\right), \tag{2.28}$$

where

$$W = -\int_{S_1}\mathbf{n}_1\cdot\mathbf{T}\cdot\mathbf{n}_1\hat{q}_1\;dA + \int_{S_2}\mathbf{n}_2\cdot\mathbf{T}\cdot\mathbf{n}_2 q_2\;dA + \int_{S_2}\tau_2^{(\alpha)}\left(\mathbf{t}_2^{(\alpha)}\cdot\mathbf{u}\right)\;dA. \tag{2.29}$$

Expression (2.28) gives the force on S_1 in the $\mathbf{e}_x$-direction due to a Navier-Stokes flow in V satisfying an appropriate set of boundary conditions on S_1 and S_2 that includes those given in (2.2)–(2.5).

To evaluate the volume integrals in (2.28) we now assume that the fluid motion is irrotational, with velocity field $\mathbf{u} = \nabla\phi$. This approximation is satisfactory when the contribution of the rotational component

of the fluid motion to the rate of change of kinetic energy and the viscous dissipation is assumed to be small in comparison with the irrotational contribution. This potential flow is obtained from the solution of the boundary-value problem (2.13)-(2.16). Clearly, such potential flow cannot satisfy, in general, the complete set of boundary conditions that the Navier-Stokes motion does satisfy. With the potential flow assumption, (2.23) for the kinetic energy yields

$$\begin{aligned}\frac{dE}{dt} &= \int_V \nabla\cdot\left[\mathbf{u}\rho\left(\frac{\partial\phi}{\partial t}+\frac{|\mathbf{u}|^2}{2}\right)\right]d\mathcal{V} = \int_V \nabla\cdot\left[\mathbf{u}\left(\rho C(t)-p\right)\right]d\mathcal{V}\\ &= -\int_{S_1}(-p)\mathbf{n}_1\cdot\mathbf{u}dA+\int_{S_2}(-p)\mathbf{n}_2\cdot\mathbf{u}dA\\ &= -U\int_{S_1}(-p)\mathbf{n}_1\cdot\mathbf{e}_x dA-\int_{S_1}(-p)\mathbf{n}_1\cdot\mathbf{v}dA+\int_{S_2}(-p)\mathbf{n}_2\cdot\mathbf{u}dA, \qquad (2.30)\end{aligned}$$

with (2.16) and $\nabla\cdot\mathbf{u}=0$.

Regarding the dissipation integral, denoting $\mathbf{D}=\mathbf{D}[\mathbf{u}=\nabla\phi]$, one can readily show that for irrotational motion the following result holds

$$\begin{aligned}\int_V 2\mu\mathbf{D}:\mathbf{D}d\mathcal{V} &= -\int_{S_1}\mathbf{n}_1\cdot 2\mu\mathbf{D}\cdot\mathbf{u}dA+\int_{S_2}\mathbf{n}_2\cdot 2\mu\mathbf{D}\cdot\mathbf{u}dA\\ &= -U\int_{S_1}\mathbf{n}_1\cdot 2\mu\mathbf{D}\cdot\mathbf{e}_x dA-\int_{S_1}\mathbf{n}_1\cdot 2\mu\mathbf{D}\cdot\mathbf{v}dA+\int_{S_2}\mathbf{n}_2\cdot 2\mu\mathbf{D}\cdot\mathbf{u}dA. \qquad (2.31)\end{aligned}$$

2.3.1 Zero tangential stress on the outer boundary

Suppose the outer boundary is also a free surface. Therefore, $\tau_2^{(\alpha)}\equiv 0$ in the last integral of (2.29) for W.

The discrepancy between the nonzero irrotational shear stress and the zero shear stress that the Navier-Stokes equations must satisfy at the free surface induces a (viscous) rotational correction to the irrotational normal stress that also enters the computation of the work integrals in (2.29). In the present formulation, this extra stress is ignored. With this assumption, W in (2.29) is computed in potential flow

$$W=-\int_{S_1}\left(-p+\mathbf{n}_1\cdot 2\mu\mathbf{D}\cdot\mathbf{n}_1\right)\hat{q}_1\ dA+\int_{S_2}\left(-p+\mathbf{n}_2\cdot 2\mu\mathbf{D}\cdot\mathbf{n}_2\right)q_2\ dA, \qquad (2.32)$$

and thus the entire right-hand side of (2.28) is furnished by purely irrotational theory and a computable formula for D_1 is obtained.

In inertia-dominated problems, in which viscosity can be regarded as 'small' and perturbations of the irrotational motion are confined to narrow boundary layers, evaluating the right-hand side of (2.28) from potential flow implies that the viscous contribution to the drag, to first order in the 'small' viscosity μ, is assumed to arise solely from the rate of energy dissipation, thereby neglecting any possible first order viscous effect coming from the first and last terms in the right-hand side of (2.28).

In the particular case of $\hat{q}_1=q_2=0$, the integrals in (2.29) are annihilated and the approximation of W is not an issue. This case represents an extension to a bounded domain of the analysis carried out by Joseph, Liao and Hu[56] and Joseph and Liao[11] that applies the dissipation approximation to a non-expanding bubble translating in an unbounded domain.

Substitution of (2.30)–(2.32) into (2.28), after some algebra, yields this expression for the force on the bubble surface in the $\mathbf{e}_x$-direction according to the dissipation method,

$$\begin{aligned}D_1 &= \int_{S_1}\left(-p+\mathbf{n}_1\cdot 2\mu\mathbf{D}\cdot\mathbf{n}_1\right)\mathbf{n}_1\cdot\mathbf{e}_x dA+\frac{1}{U}\int_{S_1}\mathbf{n}_1\cdot 2\mu\mathbf{D}\cdot\mathbf{t}_1^{(\alpha)}\left(\mathbf{t}_1^{(\alpha)}\cdot\mathbf{u}\right)dA\\ &- \frac{1}{U}\int_{S_2}\mathbf{n}_2\cdot 2\mu\mathbf{D}\cdot\mathbf{t}_2^{(\alpha)}\left(\mathbf{t}_2^{(\alpha)}\cdot\mathbf{u}\right)dA. \qquad (2.33)\end{aligned}$$

To determine the force D_2 on S_2 in the $\mathbf{e}_x$-direction by the dissipation method, we follow a procedure similar to that given above for D_1, with the difference that the governing equations are transformed to a noninertial reference frame that translates with velocity $U\mathbf{e}_x$. The steps are presented in Appendix A. There, an expression for the force on S_2 with respect to the noninertial frame is written from the transformed mechanical energy equation. Then, an expression for the force D_2 with respect to the laboratory frame can be obtained by evaluating the integrals in potential flow and by employing the transformation rules that link both coordinate systems. The outlined procedure, detailed in Appendix A, gives rise to the relation

$$\begin{aligned} D_2 &= -\int_{S_2} \left(-p + \mathbf{n}_2 \cdot 2\mu\mathbf{D} \cdot \mathbf{n}_2\right) \mathbf{n}_2 \cdot \mathbf{e}_x dA + \frac{1}{U} \int_{S_2} \mathbf{n}_2 \cdot 2\mu\mathbf{D} \cdot \mathbf{t}_2^{(\alpha)} \left(\mathbf{t}_2^{(\alpha)} \cdot \mathbf{v}\right) dA \\ &- \frac{1}{U} \int_{S_1} \mathbf{n}_1 \cdot 2\mu\mathbf{D} \cdot \mathbf{t}_1^{(\alpha)} \left(\mathbf{t}_1^{(\alpha)} \cdot \mathbf{v}\right) dA. \end{aligned} \tag{2.34}$$

Next, by used of (2.33) in (2.34), with the aid of (A.23) from the self-equilibration of irrotational viscous stresses, we obtain the net force that must be applied to the liquid system in the $\mathbf{e}_x$-direction

$$-\left(D_1 + D_2\right) = -\int_{S_1} \left(-p\right) \mathbf{n}_1 \cdot \mathbf{e}_x dA + \int_{S_2} \left(-p\right) \mathbf{n}_2 \cdot \mathbf{e}_x dA. \tag{2.35}$$

Clearly, the dissipation approximation is an irrotational theory that gives rise to results that are different from those obtained from viscous potential flow in §2.2. The discrepancy between these two irrotational methods, in the case of an outer free surface, is given by the last two terms in the right-hand side of (2.33) and (2.34).

2.3.2 Irrotational tangential stress on the outer boundary

The dissipation analysis in §2.3.1 can be slightly modified to consider an outer surface on which the tangential stress is constrained to be purely irrotational, computed from the solution of the boundary-value problem (2.13)–(2.16). A motivation for this alternative outer boundary condition is discussed in §3.3. In this case, boundary condition (2.5) becomes

$$\tau_2^{(\alpha)} = \mathbf{n}_2 \cdot 2\mu\mathbf{D} \cdot \mathbf{t}_2^{(\alpha)}, \tag{2.36}$$

on S_2, where $\mathbf{D} \equiv \nabla \otimes \nabla\phi$. Thus, there is no discrepancy between the irrotational tangential stress and the tangential stress condition that the Navier-Stokes motion must satisfy. Since (2.36) holds, the normal component of the stress on S_2 is also irrotational. Therefore, with no approximation, (2.29) now takes the form

$$\begin{aligned} W &= -\int_{S_1} \mathbf{n}_1 \cdot \mathbf{T} \cdot \mathbf{n}_1 \hat{q}_1 \; dA + \int_{S_2} \left(-p + \mathbf{n}_2 \cdot 2\mu\mathbf{D} \cdot \mathbf{n}_2\right) q_2 \; dA \\ &+ \int_{S_2} \mathbf{n}_2 \cdot 2\mu\mathbf{D} \cdot \mathbf{t}_2^{(\alpha)} \left(\mathbf{t}_2^{(\alpha)} \cdot \mathbf{u}\right) dA. \end{aligned} \tag{2.37}$$

This expression is used in (2.28). The next step consists in approximating the remaining terms in the right-hand side of (2.28) for potential flow satisfying (2.13)–(2.16). By used of (2.30)–(2.31), the entire analysis thus leads to

$$D_1 = \int_{S_1} \left(-p + \mathbf{n}_1 \cdot 2\mu\mathbf{D} \cdot \mathbf{n}_1\right) \mathbf{n}_1 \cdot \mathbf{e}_x dA + \frac{1}{U} \int_{S_1} \mathbf{n}_1 \cdot 2\mu\mathbf{D} \cdot \mathbf{t}_1^{(\alpha)} \left(\mathbf{t}_1^{(\alpha)} \cdot \mathbf{u}\right) dA. \tag{2.38}$$

The force D_2 on the outer boundary S_2 is obtained by direct integration of the (irrotational) stresses using the fact that the viscous irrotational stresses are self-equilibrated on any closed surface (Appendix B). Thus,

$$D_2 \;=\; -\int_{S_2} (-p)\,\mathbf{n}_2 \cdot \mathbf{e}_x dA. \tag{2.39}$$

It is worth mentioning that the analysis in Appendix A would lead to a different result for the force on S_2 since the zero-tangential-stress boundary condition at the bubble surface would enter the integral analysis in the dissipation approximation giving rise to D_2. On the contrary, (2.39) is an 'exact' result obtained here from direct integration over the outer boundary where the stress is known to be irrotational. Therefore, no information from the inner boundary is needed. These formulae are used in the end of §3.3.

3 Computation of the forces from the potential flow solution

To compute the forces on the bubble interface and the outer liquid boundary by used of the formulae obtained in §2, the solution of the boundary-value problem (2.13)–(2.16) for the flow is needed. This problem was examined by Sherwood[55]. Because he considered an inviscid fluid, the forces were given solely by the irrotational pressure. Since the analysis is explanatory and for the sake of completeness, a version of Sherwood's analysis is presented here in §3.1. The resulting flow field is then used in the computation of the viscous irrotational effects that gives rise to a viscous drag.

3.1 Potential flow field

In the bubble-liquid system defined in §2.1, let R_1 be the radius of the bubble and R_2 the radius of the outer surface and let ϵ be the separation between the centers of the bubble and the outer sphere. Then, the translational velocity is $U = \dot{\epsilon}$. Recall that the center of the bubble moves along the fixed direction $\mathbf{e}_x$, and its pathline contains the center of the outer envelope, thereby defining the axis of symmetry for the flow field. According to the notation defined in §2, the bubble interface and the outer sphere are denoted as S_1 and S_2, respectively. The analysis that follows aims to predict the forces exerted by the liquid on the bubble and the outer container along $\mathbf{e}_x$ for $\epsilon = 0$. The analysis is thus carried out for $\epsilon/R_1 \ll 1$ and $\epsilon/R_1 \ll R_2/R_1 - 1$.

The volume occupied by the liquid for all time is $4\pi(R_2^3 - R_1^3)/3$. Then,

$$R_1^2 \dot{R}_1 = R_2^2 \dot{R}_2, \tag{3.1}$$

where the 'dot' denotes time differentiation. Using spherical polar coordinates (r, θ) with orthonormal basis $\{\mathbf{e}_r, \mathbf{e}_\theta\}$, and the center of S_2 given by $r = 0$, the bubble surface is described by

$$r = \epsilon \cos\theta + R_1 \left[1 - \left(\frac{\epsilon}{R_1}\right)^2 \sin^2\theta\right]^{1/2}. \tag{3.2}$$

Expanding around $\epsilon = 0$,

$$r = R_1 + \epsilon \cos\theta + O(\epsilon^2). \tag{3.3}$$

The harmonics velocity potential ϕ that gives rise to an axisymmetric flow field is

$$\phi = \frac{B_0}{r} + \sum_{l=1}^{\infty} \left(A_l r^l + B_l r^{-l-1} \right) P_l(\cos\theta), \tag{3.4}$$

such that $\mathbf{u} = \nabla\phi$. In (3.4), P_l denotes the Legendre polynomial of degree l (see Strauss[57], p. 275). This potential must satisfy the boundary conditions,

$$\mathbf{n}_1 \cdot \nabla\phi\big|_{S_1} = q_1 = U\mathbf{n}_1 \cdot \mathbf{e}_x + \hat{q}_1 = \dot{R}_1 + \dot{\epsilon}\cos\,\theta - \frac{\epsilon\dot{\epsilon}}{R_1}\sin^2\theta + O\left(\epsilon^2\right), \tag{3.5}$$

and

$$\mathbf{n}_2 \cdot \nabla\phi\big|_{S_2} = q_2 = \dot{R}_2, \tag{3.6}$$

where $\hat{q}_1 = \dot{R}_1$ and, to first order in ϵ,

$$\mathbf{n}_1 = \mathbf{e}_r + \mathbf{e}_\theta \frac{\epsilon}{R_1}\sin\theta, \tag{3.7}$$

and $\mathbf{n}_2 = \mathbf{e}_r$. Condition (3.6) yields

$$B_0 = -R_2^2\dot{R}_2 = -R_1^2\dot{R}_1, \tag{3.8}$$

and

$$A_l l R_2^{l-1} = B_l(l+1)R_2^{-l-2} \quad \text{for} \quad l \geqslant 1. \tag{3.9}$$

With potential (3.4), the velocity field components in the (r,θ) frame are obtained, $\mathbf{u} = \mathbf{e}_r u_r + \mathbf{e}_\theta u_\theta = \mathbf{e}_r\partial\phi/\partial r + \mathbf{e}_\theta\partial\phi/r\partial\theta$,

Turning to the bubble surface S_1, boundary condition (3.5) allows us to find the coefficients in (3.4). In so doing, it is convenient to expand these coefficients as a power series in ϵ. That is,

$$A_l = A_l^{(0)} + A_l^{(1)}\epsilon + A_l^{(2)}\epsilon^2 + \cdots, \qquad B_l = B_l^{(0)} + B_l^{(1)}\epsilon + B_l^{(2)}\epsilon^2 + \cdots, \tag{3.10}$$

for $l \geqslant 1$, where $A_l^{(j)}$ and $B_l^{(j)}$ are related through (3.9). Sherwood[55] obtained, for $l = 1$,

$$A_1 = -\frac{R_1^3(\dot{\epsilon} + 2\epsilon\dot{R}_1R_1^{-1})}{R_2^3 - R_1^3}, \qquad B_1 = -\frac{R_1^3R_2^3(\dot{\epsilon} + 2\epsilon\dot{R}_1R_1^{-1})}{2(R_2^3 - R_1^3)}, \tag{3.11}$$

to first order in ϵ. Some detail on the computations of these coefficients by imposing constraint (3.5) is given in Appendix C, where expressions for A_2 and B_2 to leading order are presented as well. There, we also show that $A_l^{(0)} = B_l^{(0)} = 0$ for $l \geqslant 2$ and that $A_l^{(1)} = B_l^{(1)} = 0$ for $l \geqslant 3$. Since the forces on S_1 and S_2 in the $\mathbf{e}_x$-direction are computed for $\epsilon = 0$, it suffices to find the coefficients B_0, A_1, B_1, A_2 and B_2 to first order in ϵ and then calculate their time derivatives. These computations will show, however, that only $l = 1$ terms—and thus A_1 and B_1—are actually needed because of orthogonality properties of Legendre polynomials.

The fluid pressure p distribution on S_1 and S_2 can be obtained from Bernoulli equation (2.16). The derivative $\partial\phi/\partial t$ needed to compute p is obtained from (3.4) by differentiating the coefficients and then putting $\epsilon = 0$, with $r = R_1$ or $r = R_2$.

Using standard formulae, the components of the strain-rate tensor in spherical-polar coordinates can be computed from $\mathbf{u} = \nabla\phi$, with ϕ given in (3.4). These computations yield

$$D_{rr} = \mathbf{e}_r \cdot 2\mu\mathbf{D}[\nabla\phi]\cdot\mathbf{e}_r = \sum_{l=0}^{\infty}\left[l(l-1)A_l r^{l-2} + (l+1)(l+2)B_l r^{-l-3}\right]P_l(\cos\theta), \tag{3.12}$$

$$D_{r\theta} = \mathbf{e}_r \cdot 2\mu\mathbf{D}[\nabla\phi]\cdot\mathbf{e}_\theta = \sum_{l=1}^{\infty}\left[(l-1)A_l r^{l-2} - (l+2)B_l r^{-l-3}\right]dP_l(\cos\theta)/d\theta. \tag{3.13}$$

For $\epsilon = 0$, at $r = R_1$, the velocity component u_r is given by (3.5) and the component $u_\theta = \partial\phi/r\partial\theta$; hence,

$$u_r = \dot{R}_1 + \dot{\epsilon}\cos\theta, \qquad u_\theta = -\left(A_1 + B_1 R_1^{-3}\right)\sin\theta. \tag{3.14}$$

At $r = R_2$, with $\epsilon = 0$, $u_r = \partial\phi/\partial r$ and $u_\theta = \partial\phi/r\partial\theta$ give

$$u_r = -B_0 R_2^{-2}, \qquad u_\theta = -\left(A_1 + B_1 R_2^{-3}\right)\sin\theta. \tag{3.15}$$

With $\epsilon = 0$, evaluating (3.12) and (3.13) at $r = R_1$ yields

$$D_{rr} = 2B_0 R_1^{-3} + 6B_1 R_1^{-4}\cos\theta, \qquad D_{r\theta} = 3B_1 R_1^{-4}\sin\theta, \tag{3.16}$$

and, at $r = R_2$, we have

$$D_{rr} = 2B_0 R_2^{-3} + 6B_1 R_2^{-4}\cos\theta, \qquad D_{r\theta} = 3B_1 R_2^{-4}\sin\theta. \tag{3.17}$$

In these results, B_0 is given by (3.8) and A_1 and B_1 are given in (3.11) with $\epsilon = 0$. It is worth noting that the alternative approach of computing the velocity potential from a boundary-value problem that considers two instantaneously growing or collapsing concentric spheres would have sufficed to obtain the strain-rate tensor $\mathbf{D}[\nabla\phi]$, since it only involves spatial partial differentiation.

Below, the forces on the bubble interface S_1 and the outer boundary S_2 are computed from the formulae of this section and §2 for $\epsilon = 0$. When the bubble and the outer surface are concentric, $\mathbf{n}_1 = \mathbf{n}_2 = \mathbf{e}_r$, $\mathbf{t}_1 = \mathbf{t}_2 = \mathbf{e}_\theta$, with $\mathbf{e}_r\cdot\mathbf{e}_x = \cos\theta$ and $\mathbf{e}_\theta\cdot\mathbf{e}_x = -\sin\theta$.

3.2 Forces—Viscous potential flow

The force on the bubble according to viscous potential flow is computed from (2.18). For the spherical bubble, with $\epsilon = 0$ at $r = R_1$, this expression becomes,

$$D_1 = 2\pi R_1^2\int_0^\pi \left(-p + 2\mu D_{rr}\right)\big|_{R_1}\cos\theta\sin\theta d\theta. \tag{3.18}$$

With Bernoulli equation (2.16), computing $\partial\phi/\partial t$, and using (3.14) and (3.16), we get

$$D_1 = -\frac{4}{3}\pi\rho R_1^3\left[\frac{\ddot{\epsilon}(2R_1^3 + R_2^3)}{2(R_2^3 - R_1^3)} + \frac{\dot{\epsilon}\dot{R}_1(15R_1^3 + 3R_2^3)}{2R_1(R_2^3 - R_1^3)} + \frac{6\nu\dot{\epsilon}}{R_1^2}\frac{R_2^3}{(R_2^3 - R_1^3)}\right]. \tag{3.19}$$

Taking $R_2 \to \infty$, this expression leads to

$$D_1 = -\frac{4}{3}\pi\rho R_1^3\left[\frac{\ddot{\epsilon}}{2} + \frac{3\dot{\epsilon}\dot{R}_1}{2R_1} + \frac{6\nu\dot{\epsilon}}{R_1^2}\right]. \tag{3.20}$$

In particular, for a spherical bubble of constant volume that translates with constant velocity (i.e. $\dot{R}_1 = 0$ and $\ddot{\epsilon} = 0$), (3.20) reduces to $D_1 = -8\pi\mu\dot{\epsilon}R_1$ a result found by Moore (1959) from direct

integration of the viscous normal stress in irrotational motion. If the fluid is considered inviscid, then the drag is zero (d'Alembert's paradox). When the acceleration $\ddot{\epsilon}$ is not zero, (3.20) gives rise to the apparent-mass.

With $\dot{R}_1 = 0$ and the void fraction $\alpha = (R_1/R_2)^3$, (3.19) reduces to

$$D_1 = -\frac{4}{3}\pi\rho R_1^3 \left[\frac{\ddot{\epsilon}(1+2\alpha)}{2(1-\alpha)} + \frac{6\nu\dot{\epsilon}}{R_1^2}\frac{1}{(1-\alpha)}\right], \tag{3.21}$$

in agreement, when $\nu = 0$, with (AI.11) of Zuber[58] for the force on a spherical bubble moving within a inviscid liquid bounded by a spherical shell. This leads to the cell void fraction correction of the accelerated-apparent mass given in (3.20).

For 'small' α, it is useful to write (3.21) in the form

$$D_1 = -\frac{4}{3}\pi\rho R_1^3 \left[\frac{\ddot{\epsilon}}{2}(1+3\alpha) + \frac{6\nu\dot{\epsilon}}{R_1^2}(1+\alpha)\right] + O(\alpha^2). \tag{3.22}$$

The force on the outer sphere, $r = R_2$, with $\epsilon = 0$, is obtained from (2.19) when the outer boundary is a free surface. This yields,

$$D_2 = -2\pi R_2^2 \int_0^\pi (-p + 2\mu D_{rr})\,\big|_{R_2} \cos\theta \sin\theta d\theta. \tag{3.23}$$

Finding $\partial\phi/\partial t$, with (3.15) and (3.17), this formula gives,

$$D_2 = \frac{4}{3}\pi\rho R_2^3 \left[\frac{3\ddot{\epsilon}R_1^3}{2(R_2^3 - R_1^3)} + \frac{\dot{\epsilon}R_1^2\dot{R}_1(15R_2^3 + 3R_1^3)}{2R_2^3(R_2^3 - R_1^3)} + \frac{6\nu\dot{\epsilon}}{R_2^2}\frac{R_1^3}{(R_2^3 - R_1^3)}\right]. \tag{3.24}$$

Using (3.19) and (3.24), the total force that must be applied to the system is

$$-(D_1 + D_2) = -\frac{4}{3}\pi\rho R_1^3 \left[\ddot{\epsilon} + \frac{6\dot{\epsilon}\dot{R}_1}{R_1} - \frac{6\nu\dot{\epsilon}}{R_1^2}\frac{R_2(R_2^2 - R_1^2)}{(R_2^3 - R_1^3)}\right]. \tag{3.25}$$

For $\nu = 0$ (inviscid fluid), these results reduce to those obtained by Sherwood[55]. The force D_2 when the irrotational stress is specified on S_2 is given by (3.24) with $\nu = 0$. This follows from (2.22).

3.3 Forces—Dissipation method

The force D_1 on the bubble interface S_1 in the $\mathbf{e}_x$-direction can be obtained by used of (2.33) when a zero shear stress is prescribed on the outer boundary. This formula can be written as,

$$\begin{aligned} D_1 &= 2\pi R_1^2 \int_0^\pi (-p + 2\mu D_{rr})\,\big|_{R_1} \cos\theta \sin\theta d\theta + \frac{2\pi R_1^2}{\dot{\epsilon}} \int_0^\pi (2\mu D_{r\theta} u_\theta)\,\big|_{R_1} \sin\theta d\theta \\ &- \frac{2\pi R_2^2}{\dot{\epsilon}} \int_0^\pi (2\mu D_{r\theta} u_\theta)\,\big|_{R_2} \sin\theta d\theta. \end{aligned} \tag{3.26}$$

With (2.16) for the pressure, (3.14) and (3.16), (3.26) leads to

$$D_1 = -\frac{4}{3}\pi\rho R_1^3 \left[\frac{\ddot{\epsilon}(2R_1^3 + R_2^3)}{2(R_2^3 - R_1^3)} + \frac{\dot{\epsilon}\dot{R}_1(15R_1^3 + 3R_2^3)}{2R_1(R_2^3 - R_1^3)} + \frac{9\nu\dot{\epsilon}}{R_1^2}\frac{R_2(R_2^5 - R_1^5)}{(R_2^3 - R_1^3)^2}\right]. \tag{3.27}$$

This expression, with $R_2 \to \infty$, reduces to

$$D_1 = -\frac{4}{3}\pi\rho R_1^3 \left[\frac{\ddot{\epsilon}}{2} + \frac{3\dot{\epsilon}\dot{R}_1}{2R_1} + \frac{9\nu\dot{\epsilon}}{R_1^2}\right]. \tag{3.28}$$

For a spherical bubble of constant volume moving with constant velocity $\dot{\epsilon}$ in an infinite fluid, (3.28) gives $D_1 = -12\pi\mu\dot{\epsilon}R_1$. This result has been obtained with the dissipation method in potential flow by several authors[8–12,14,56].

Moore[12] has examined the discrepancy between the viscous potential flow solution and the correct dissipation result for the drag over a spherical bubble of constant volume translating in an unbounded domain. Moore explains, citing an idea due to G. K. Batchelor, that the addition of an extra-pressure or viscous correction to the irrotational normal stress can compensate such discrepancy. From a boundary-layer type of analysis assessing the order of magnitude of the various terms in the steady governing equations, Moore concludes that the extra-pressure 'contributes to the drag on the bubble to the same order as the viscous stresses'[12], since he found that this extra-pressure is first order in the dimensionless viscosity. If the extra-pressure produces work, this is evidently neglected in the approach used here (that is, for nonzero choices of $\hat{q}_1$ and q_2), for W in (2.29) is approximated by the irrotational pressure and irrotational viscous normal stress.

For a bubble of variable radius in an unbounded fluid, the viscous part in (3.28) can be reduced from the multiple-bubble analysis by Voinov and Golovin[25]. They applied a Lagrangian formulation to examine the motion of a set of N bubbles of varying radius translating in a liquid otherwise at rest with dissipative forces computed from the rate of viscous dissipation evaluated in potential flow. Magnaudet and Legendre[18] obtained (3.28) by transforming the original problem to a reference frame in which the bubble radius remains fixed, while preserving the dynamic similarity in the transformation. In the limit when $Re >> 1$ or $\mathcal{U}Re >> 1$, where the Reynolds number $Re = R_1U/\nu$ and the velocity ratio $\mathcal{U} = |\dot{R}_1|/U$, the boundary layer is thin. The transformed problem thus involves a bubble of constant radius in an unsteady flow and the drag force is computed to first order in the viscosity by evaluating the kinetic energy and the viscous dissipation from potential flow (see Tam[16]). Then, the force in physical space is found by simply applying the known rules that link the transformed problem to the original one. This method contrasts with the approach described in §2.3 that gives rise to (3.28), in which the work of the normal stress due to the radial motion of the bubble interface and the contribution of this motion to the liquid kinetic energy are modeled by potential flow in a rather heuristic way. The fact that (3.28) agrees with the force given by Magnaudet and Legendre (1998) indicates that the combined viscous contribution from dE/dt and W in (2.28) is null up to order $O(Re^{-1})$. This may be explained by considering that the component of the total motion attributed to the bubble radial expansion and contraction is of the source-sink type, hence of irrotational nature.

The result obtained above can be readily used to approximate the dynamics in a bubbly flow with void fraction α by applying the cell model described in §1. In the case of $\dot{R}_1 = 0$, with the cell void fraction $\alpha = (R_1/R_2)^3$, (3.27) gives the added-mass and viscous contributions to the force acting on each bubble

$$D_1 = -\frac{4}{3}\pi\rho R_1^3\left[\frac{\ddot{\epsilon}(1+2\alpha)}{2(1-\alpha)} + \frac{9\nu\dot{\epsilon}}{R_1^2}\frac{(1-\alpha^{5/3})}{(1-\alpha)^2}\right], \tag{3.29}$$

which agrees with Zuber's[58] result for $\nu = 0$. The viscous part in (3.29) is the widely cited result obtained with the dissipation approximation by Marrucci[51]. For 'small' α, (3.29) may be written as

$$D_1 = -\frac{4}{3}\pi\rho R_1^3\left[\frac{\ddot{\epsilon}}{2}(1+3\alpha) + \frac{9\nu\dot{\epsilon}}{R_1^2}(1+2\alpha)\right] + O(\alpha^2). \tag{3.30}$$

It should be noted that (3.29) has been derived from a cell model with a frictionless outer boundary, such that no work is exchanged by the reference cell with the surroundings.

The force D_2 in the $\mathbf{e}_x$-direction on surface S_2 can be obtained from either (2.34) or (2.35). The latter expression can be written as

$$D_1 + D_2 = 2\pi R_1^2\int_0^\pi (-p)\,\big|_{R_1}\cos\theta\sin\theta d\theta - 2\pi R_2^2\int_0^\pi (-p)\,\big|_{R_2}\cos\theta\sin\theta d\theta, \tag{3.31}$$

which, with (3.27), leads to

$$D_2 = \frac{4}{3}\pi\rho R_2^3\left[\frac{3\ddot{\epsilon}R_1^3}{2(R_2^3-R_1^3)} + \frac{\dot{\epsilon}R_1^2\dot{R}_1(15R_2^3+3R_1^3)}{2R_2^3(R_2^3-R_1^3)} + \frac{9\nu\dot{\epsilon}}{R_2^2}\frac{R_1(R_2^5-R_1^5)}{(R_2^3-R_1^3)^2}\right]. \tag{3.32}$$

Again, Sherwood's results are recovered taking $\nu = 0$ in (3.27) and (3.32).

The total force that must be applied to the system is obtained from (3.31):

$$-(D_1+D_2) = -\frac{4}{3}\pi\rho R_1^3\left(\ddot{\epsilon} + \frac{6\dot{\epsilon}\dot{R}_1}{R_1}\right), \tag{3.33}$$

in agreement with the inviscid result by Sherwood[55].

Consider now an outer boundary S_2 in which the tangential stress is given by the irrotational motion satisfying the boundary-value problem (2.13)-(2.16), such that the zero-tangential-stress constraint does not hold. Under this framework, the formulae of §2.3.2 can be applied yielding an expression for the force D_1 on the bubble and the force D_2 on the outer spherical envelope. Applying (2.38), we obtain,

$$D_1 = -\frac{4}{3}\pi\rho R_1^3\left[\frac{\ddot{\epsilon}(2R_1^3+R_2^3)}{2(R_2^3-R_1^3)} + \frac{\dot{\epsilon}\dot{R}_1(15R_1^3+3R_2^3)}{2R_1(R_2^3-R_1^3)} + \frac{9\nu\dot{\epsilon}}{R_1^2}\frac{R_2^6}{(R_2^3-R_1^3)^2}\right]. \tag{3.34}$$

With $\dot{R}_1 = 0$, in terms of the void fraction α, this expression becomes,

$$D_1 = -\frac{4}{3}\pi\rho R_1^3\left[\frac{\ddot{\epsilon}(1+2\alpha)}{2(1-\alpha)} + \frac{9\nu\dot{\epsilon}}{R_1^2}\frac{1}{(1-\alpha)^2}\right]. \tag{3.35}$$

To first order in α, (3.35) also leads to (3.30). The viscous part of (3.35) has been given by Kendoush[52], as discussed below. The force D_2, according to (2.39), can be obtained from either (3.24) or (3.32) taking $\nu = 0$. For the two outer boundary conditions examined here, note that the force on the bubble increases with the void fraction according to both irrotational theories.

4 Discussion

The force acting on a spherical compressible bubble in rectilinear motion within an incompressible fluid bounded externally by a spherical surface has been computed above at the instant in which both spheres are concentric. The analysis is carried out using two different irrotational approximations, namely, viscous potential flow (§§2.2 and 3.2), which directly integrates the irrotational normal stress over the bubble surface, and the dissipation method (§§2.3 and 3.3), in which the integration of the various terms in the mechanical energy equation, including the rate of energy dissipation, is carried out assuming irrotational motion, after satisfying actual boundary conditions for Navier-Stokes motion. The dissipation method stems from the fact that viscous irrotational stresses are self-equilibrated, but its power does not vanish[59]. In addition, the force on the outer surface is also computed. In particular, by keeping the bubble radius constant, one can use the results to approach the force on a bubble moving in a monodispersed homogeneous bubbly flow having the same void fraction as the reference cell and satisfying the dual limit of large Reynolds and small Weber numbers, for in this case the velocity field differs very little from that in irrotational motion. This is in accord with the well-known cell-model approximation.

In the present formulation of the dissipation method, the tangential stress is set to zero on the inner boundary, but two possibilities are considered for the outer boundary, either a zero tangential stress or an irrotational tangential stress. Since the irrotational tangential stress on the outer boundary is not identically zero, this stress does work against the remainder of the domain, as shown in (2.37). This

boundary condition thus contradicts the postulate by Happel and Brenner[45] of regarding each cell as an independent entity in the sense that energy transfer should not occur between the unit cell and the neighboring fluid. This is the case with the model with zero tangential stress on both the inner and outer boundaries (i.e. free-surface cell model), leading to Marrucci's drag when the bubble speed is constant. Nevertheless, if the cell model is used to describe a bubbly flow with 'weak' rotational effects confined to a thin layer adjacent to the bubble interface and a minute wake at the bubble rear, such that the liquid motion is essentially irrotational, the choice of irrotational stresses on the outer envelope appears reasonable.

The viscous drag from the viscous potential flow solution (3.21) is always lower than the viscous drag obtained from the dissipation method with either outer boundary condition, (3.29) or (3.35), for the same volume fraction α. It is well known[12] that the drag on a single bubble rising steadily in a liquid from the integration of the viscous irrotational normal stress (i.e. viscous potential flow in this paper) is 2/3 of that predicted by the dissipation method, which gives the correct trend for a large-Reynolds-number spherical bubble. Therefore, one may expect the results from the dissipation method to be closer to the actual viscous drag than those from viscous potential flow for nonzero α.

For a bubble moving with constant velocity, i.e. $\ddot{\epsilon} = 0$, (3.35) reduces to the drag found by Kendoush[52] with the dissipation method using a cell model. Nonetheless, in his analysis, it is not stated what dynamic constraint (stress) is prescribed at the outer boundary. Expressions (3.34) and hence (3.35) were attained here by imposing an irrotational tangential stress on the outer boundary. Both Marruci[51] and Kendoush[52] used the irrotational velocity profile determined by the domain configuration and the kinematic conditions (normal velocity component) on the inner and outer boundaries. Kendoush's working equation [his (5)] can be obtained from (2.38) by used of (2.1).

Kendoush also argues that Marrucci's result, given in (3.29) for $\ddot{\epsilon} = 0$, is incorrect, reasoning that the upper integration limit in Marrucci's dissipation integral should have been taken to infinity instead of using the outer radius, as originally specified by Marrucci. Although implementing this change in Marrucci's formulation does lead to (3.35) instead of (3.29), we find this modification rather contradictory since in the cell model the liquid is bounded, and the velocity profile employed is that of a confined fluid. The analysis that led to (3.29) verifies that Marrucci's formula for the viscous drag is correct; it is found here from the mechanical energy balance by considering frictionless inner and outer boundaries and irrotational motion in the bulk of fluid. It should be noted that Marrucci did not prescribe any external boundary condition from dynamics (i.e. stress), although he mentioned Happel's[48] assumption of a free-surface condition for the outer boundary in a creeping-flow cell model as a prominent antecedent of his work. He only indicates that boundary-layers contributions to the total energy dissipation are neglected in his analysis.

While a zero tangential stress is the obvious choice for the bubble interface, an alternative constraint, that is, an irrotational stress condition, may be specified on the outer boundary. In sum, (3.29) and (3.35) arise through the dissipation method applied to the same configuration with the same frictionless condition on the inner boundary but each satisfying a different condition on the outer boundary, thereby yielding different results. Nonetheless, the drag is the same to first order in the void fraction.

4.1 Comparison with numerical and other analytical results

The viscous irrotational theories considered here can be compared with results from other analytical models, numerical simulations and experimental data. We have in mind the situation of gas being bubbled through a stagnant liquid in a continuous manner by injecting a constant gas flow rate or the case of a swarm of spherical bubbles rising by buoyancy in a liquid otherwise at rest. The latter case can be placed in the framework of the cell-model analysis carried out here by letting U be the velocity of the rising bubble swarm with respect to the container wall[51,53]. If a steady gas flow rate is bubbled through the same container, the actual bubble velocity U_b referred to the container walls is related to U by the

expression $U_b = U/(1-\alpha)$ as a result of mass conservation[60], where α is also the gas volume fraction in the bubbly flow. In this case, U also represents the gas drift velocity, that is, the difference of the actual gas velocity, U_b, and the gas volumetric flow rate per unit of cross sectional area being pushed into the system[60]. It is assumed that the bubbles in the swarm are nearly spherical, homogeneously distributed, and with negligible variations of the equivalent bubble diameter with respect to the mean value. The equivalent bubble diameter is the diameter of the sphere with the same volume of the bubble. We are referring to this definition when we use the term 'bubble diameter'.

In Figure 2(a) the predictions by the irrotational theories for the drag coefficient C_D are presented and compared with those listed in Chhabra[46] from the numerical solution of the steady incompressible Navier-Stokes equations using both the free-surface and the zero-vorticity cell-model approximations for $Re = 100$, where $Re = 2R_1U\rho/\mu$, thereby suitable for comparison with the viscous irrotational theories. Numerical results for $Re = 20$ are also included to illustrate the change in C_D with Re. Chhabra collected the results obtained by Manjunath *et al.*[54] using the finite-element method for a cell model with zero tangential stress both on the inner and outer boundary and new results generated with the same numerical method solving the governing equations for the same physical domain and boundary conditions except that at the outer boundary the vorticity is set to zero instead of the tangential stress. The drag D on a bubble may be written in the form

$$D = \frac{1}{2}\rho U^2 \pi R_1^2 C_D, \tag{4.1}$$

an expression that defines the drag coefficient C_D. Using the results for the viscous drag from (3.21), (3.29) and (3.35), expressions for the drag coefficient can thus be written, respectively, for viscous potential flow (VPF) and the dissipation method (DM) with either a zero tangential stress or an irrotational tangential stress on the outer boundary. In this order, we obtain,

$$C_{D_1} = \frac{32}{Re}\frac{1}{(1-\alpha)}, \qquad C_{D_2} = \frac{48}{Re}\frac{(1-\alpha^{5/3})}{(1-\alpha)^2}, \qquad C_{D_3} = \frac{48}{Re}\frac{1}{(1-\alpha)^2}. \tag{4.2.a, b, c}$$

Figure 2(a) shows that the DM with the irrotational-tangential-stress condition on the outer boundary exhibits fair agreement with the numerical results for the zero-vorticity cell model for the range of void fraction considered in the study. In this formulation of the dissipation approximation, the potential flow hypothesis is brought from the bulk of the fluid to include the outer boundary. Predictions from the DM with the zero-tangential-stress condition on the outer surface are close to the numerical simulations using a cell model with the same constraint, as expected for $Re = 100$. VPF, on the other hand, consistently underpredicts the numerical solution, which is the extension to a bubbly suspension of the known result for a single bubble rising in an infinite medium[12]. From the two curves rendered by DM, the cell model with an irrotational shear stress on the outer boundary predicts values for the drag coefficient C_D that display a stronger dependence on the void fraction than those from the cell model with a zero-shear-stress condition. A similar trend is described by the numerical results by Chhabra, who commented on this, for $Re = 100$ (represented by symbols), that is, results from the zero-vorticity cell model are more dependent upon the void fraction than results from the free-surface cell model. This trend agrees with that reported by Happel and Brenner[45] and El-Kaissy and Homsy[50]. Happel and Brenner framed their discussion under the analysis of creeping flow; El-Kaissy and Homsy carried out regular perturbation techniques on the Navier-Stokes equations. A comparison of numerical predictions for the drag coefficient with Marrucci's drag [cf. (4.2.b)] has been presented by Manjunath *et al.* using the free-surface cell model.

Although numerical simulations and analytical models can predict the drag acting on a bubble in a bubbly suspension, perhaps the most convenient way of evaluating their performance is comparing theoretical results for the terminal rise velocity of the bubbles with experimental data. This is because

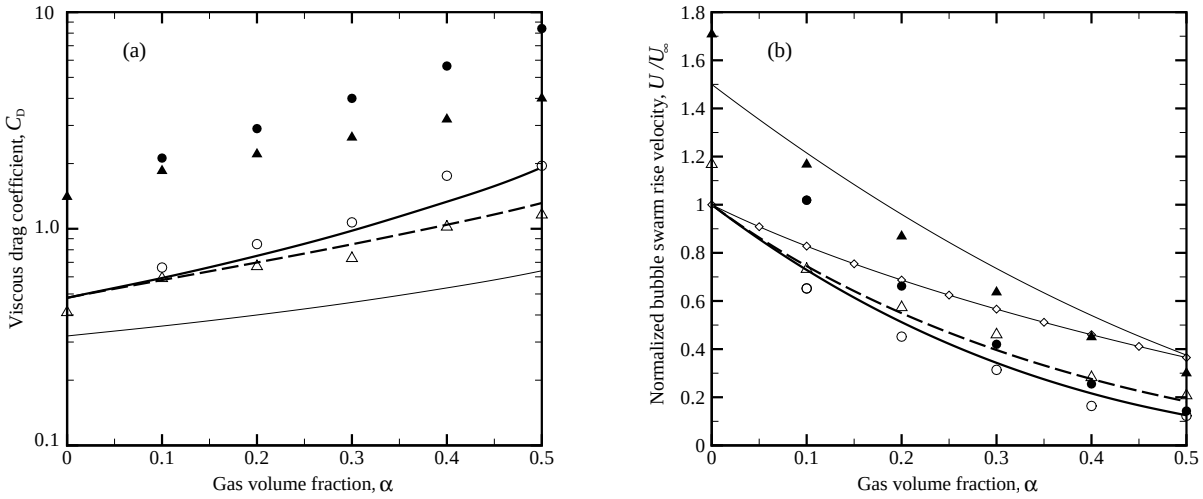

Figure 2: (a) Drag coefficient C_{D} as a function of the void fraction α. (b) Normalized bubble swarm rise velocity U/U_∞ as a function of the gas volume fraction α. The graphs for C_{D} vs. α are determined with Re=100, except where indicated. The curves of U/U_∞ vs. α are valid for $Re \gg 1$ but do not explicitly depend on Re. Thin solid line: VPF (4.2.a) and (4.3.a); thick dashed line: DM with zero tangential stress on the outer boundary (4.2.b) and (4.3.b); thick solid line: DM with irrotational tangential stress on the outer boundary (4.2.c) and (4.3.c); thin solid line with ⋄: Marrucci[51]; ▲ and △: numerical simulations with free-surface cell model by Chhabra[46] for Re=20 and Re=100, respectively, where (4.6) is used for the normalized velocity; • and ○: numerical simulations with zero-vorticity cell model by Chhabra for Re=20 and Re=100, respectively. DM stands for the dissipation method and VPF stands for viscous potential flow. The symbols for $\alpha = 0$ correspond to the numerical results by Manjunath *et al.*[54] using a free-surface cell model. U_∞ denotes the single bubble rise velocity from the dissipation method.

measurements of this magnitude are somewhat abundant in the literature. The terminal velocity U of a swarm of spherical bubbles of equal size rising due to buoyancy can be determined by equating the drag on a bubble with the lift force that drives the bubble upwards, given by the buoyancy force corrected by the bubble weight, that is, $4\pi R_1^3(\rho_{\rm M}-\rho_{\rm G})g/3$, g being the acceleration of gravity, $\rho_{\rm G}$ the gas density and $\rho_{\rm M}\equiv\rho(1-\alpha)+\rho_{\rm G}\alpha$, the averaged density of the mixture[52,58,61]. Using (3.21), (3.29) and (3.35) for the drag, we thus find,

$$\frac{U}{U_\infty}=\frac{3}{2}(1-\alpha)^2, \qquad \frac{U}{U_\infty}=\frac{(1-\alpha)^3}{(1-\alpha^{5/3})}, \qquad \frac{U}{U_\infty}=(1-\alpha)^3, \tag{4.3.a, b, c}$$

for VPF, and the DM with either a zero tangential stress or an irrotational tangential stress at the outer boundary of the cell, respectively. Here, U_∞ is the bubble velocity in the limit of infinite dilution, that is for $\alpha=0$, computed from the DM[1], $U_\infty=R_1^2(\rho-\rho_{\rm G})g/9\mu$. Hence the bubble rise velocity for infinite dilution according to VPF is $3U_\infty/2$. Expression (4.3.c) has been given by Kendoush[52]. Expression (4.3.b) times the factor $(1-\alpha)^{-1}$ gives the rise velocity model by Marrucci[51], who apparently used the density of the liquid ρ instead of the density of the mixture $\rho_{\rm M}$ in the buoyancy force. Richardson and Zaki[62] favored the use of the density of the liquid over the density of the suspension $\rho_{\rm M}$ in computing the buoyancy force acting on solid particles settling in a liquid at the same rate, pointing out that each particle displaces its own volume of liquid, not of suspension. Kuwabara[49] also used the density of the liquid instead of that of the suspension for the buoyancy force needed in the evaluation of the terminal settling velocity of spheres uniformly arranged in a liquid. Manjunath *et al.* proposed to compute the steady rise velocity of the bubble swarm with the buoyancy force determined by the density of the liquid. On the other hand, Zuber[58] applied the one-dimensional momentum equation for two-phase flow to the case of steady vertical motion of particles in a fluid neglecting the friction at the walls, finding that the buoyancy force determined with the density of the mixture balances the drag force on a particle and its weight. Based upon experimental studies on the settling velocity of spheres in two-component solid-liquid suspensions, Poletto and Joseph[63] affirmed that the effective density approaches the average density of the mixture in the case of a test particle of the same diameter as the suspended particles, or larger. Moreover, they entered the average density of the mixture to account for the effective buoyancy on a test particle in a model describing the settling of a test sphere in a suspension. Kendoush also used the density of the mixture in finding the terminal rise velocity of a bubble swarm. This approach was adopted above.

Expressions (4.3.a, b, c) are plotted in figure 2(b) as function of the void fraction. To use the numerical results for $C_{\rm D}$ compiled in Chhabra for fixed Reynolds number Re and varying α to predict the ratio U/U_∞, the drag D in (4.1) is equated to the buoyancy force minus the bubble weight. That is,

$$C_{\rm D}\frac{1}{2}\rho U^2\pi R_1^2=\frac{4}{3}\pi R_1^3(\rho-\rho_{\rm G})g(1-\alpha). \tag{4.4}$$

Writing a similar expression in the infinite dilution limit, $\alpha=0$, for a bubble of radius R_1 rising with velocity U_∞ in the same liquid, according to the dissipation method, the drag coefficient being $C_{{\rm D},\infty}$, and combining with (4.4), we find[64]

$$\frac{U}{U_\infty}=(1-\alpha)^{1/2}\left(\frac{C_{{\rm D},\infty}}{C_{\rm D}}\right)^{1/2}. \tag{4.5}$$

With $C_{{\rm D},\infty}$ given by the known expression $C_{{\rm D},\infty}=48/Re_\infty$, and $U/U_\infty=Re/Re_\infty$, (4.5) represents and implicit relation for Re_∞, for known values of α and Re, a pair that determines the drag coefficient $C_{\rm D}$ from the numerical analysis. Expression (4.5) can be written in explicit form,

$$\frac{U}{U_\infty}=(1-\alpha)\frac{48}{ReC_{\rm D}} \tag{4.6}$$

The results from (4.6) for Re=20 and 100 are represented with symbols in figure 2(b).

The trend depicted by the viscous irrotational theories in figure 2(b) indicates a decrease in the ratio U/U_∞ for the bubble swarm with increasing void fraction. For a given gas-liquid system for which the dual limit of large Reynolds number and small Weber number is satisfied, this trend indicates that increasing bubble concentration hinders the bubble swarm rise speed. DM with an irrotational tangential stress on the outer boundary of the cell model gives the lowest normalized velocity amongst the irrotational theories described in this paper. Slightly higher values are obtained from the DM when a zero tangential stress is prescribed on the outer boundary for the same volume fraction. In addition, results from the former model are somewhat more dependent on the void fraction than results from the latter model. VPF predicts much higher normalized bubble swarm velocities than the other models considered in the analysis as the first order viscous correction to the irrotational pressure associated with the vortical layer is omitted, thereby predicting a lower drag. Marrucci's formula predicts dimensionless velocities that lie in between those from VPF and the other viscous irrotational theories and shows a less pronounced dependence on the gas volume fraction.

The results obtained here (plotted as symbols) from the drag coefficients reported in Chhabra from numerical simulations also show a decrease in U/U_∞ as the void fraction α increases. In the limit of infinite dilution, the points included in figure 2(b) are given in Manjunath *et al.* from their numerical solution. The remark stated above regarding the hindering effect due to increasing gas concentration cannot be drawn from the points determined by the numerical solution, as each data series corresponds to a fixed bubble swarm Reynolds number, Re. Since (4.6) with the numerical results for C_D in Chhabra for $Re = 20$ and 100 yields an increasing Re_∞ as α increases, the ratio Re/Re_∞ and hence U/U_∞ ought to decrease. To investigate the effect of increasing gas volume concentration on bubble rise velocity using numerical simulations at finite Reynolds number, another type of plot is needed; this can be found elsewhere[52,53](see below). For both Re =20 and 100 and $\alpha > 0$, the normalized velocity predictions from the free-surface cell model are larger than the results from the zero-vorticity cell model obtained by means of computational fluid dynamics analysis. As expected, this trend agrees with that shown by the DM results for U/U_∞ with the zero-tangential-stress model leading to a somewhat larger values in comparison with the model with an irrotational tangential stress on the exterior surface. Larger values of U/U_∞ are predicted for bubble swarms for which $Re = 20$ than for swarms with $Re = 100$ at a fixed gas volume fraction and for the same type of cell model. The difference between both series decreases as the gas volume fraction increases.

The decrease of the normalized bubble swarm velocity U/U_∞ as Re increases for fixed α may be explained by considering the limit of low Reynolds number. For creeping motion of a single bubble in an unbounded medium, the drag is known[65] to be $4\pi\mu R_1 U$. Therefore, the bubble terminal rise velocity is U/U_∞=3, which is well above the corresponding value for $Re = 20$, $U/U_\infty \approx$1.7 [see figure 2(b)]. As the Reynolds number increases towards the other limit $Re \gg 1$, U/U_∞ should tend to 1. This tendency is also observed for a bubble swarm, that is, for $\alpha > 0$.

As the Reynolds number increases, it is reasonable to expect that U/U_∞ for given α approaches the curves resulting from the DM, since these curves represent the limiting values for $Re \gg 1$. Whereas for $\alpha = 0$ and $Re = 100$, $U/U_\infty \approx 1.2$, and a decreasing trend should be expected, so that $U/U_\infty \to 1$ as Re increases, the data obtained from numerical experiments for $\alpha > 0$ using the free-surface cell model apparently have already reached their limit, given by the DM analysis for the same type of cell model. In the case of the data set corresponding to the zero-vorticity cell model, for $\alpha > 0$ the magnitudes of U/U_∞ are already slightly under their expected limiting values, the graph of the DM with an irrotational tangential stress on the exterior boundary. Discarding issues related to the approximations employed in the numerical scheme, one possible explanation for this result is the increasing trend of the product ReC_D with increasing Re that, by virtue of (4.6), leads to a decrease in U/U_∞. Should this trend be reversed, ReC_D would start decreasing slowly as Re continues increasing so that the limiting value would be closely approached, and U/U_∞ would become insensitive to changes in Re.

In closing, one should mention that results for $U/U_{\alpha=0}$ as function of the gas volume fraction, $U_{\alpha=0}$ being the velocity of a bubble rising in an unbounded medium ($U_{\alpha=0} \neq U_\infty$), were reported by LeClair and Hamielec[53] for infinite dilution Reynolds numbers up to $Re_{\alpha=0}$=1000 from their numerical solutions employing the zero-vorticity cell model. There, the hindering of bubble motion as the bubble concentration increases is demonstrated from the simulations. They pointed out that a standing vortex ring in the bubble rear stagnation region was not present. They assert that for such a high Reynolds number, the limit given by potential flow theory is approached. From the dissipation method, the drag coefficient defined in (4.1) leads to the result $C_\mathrm{D} \approx 0.048$ yet they plotted a drag coefficient, defined in the same manner, of $C_\mathrm{D} \approx 0.1$. Appreciable covective effects that overcome the capabilities of the numerical scheme[66] are perhaps the cause of such a significant difference. Therefore, we opted not to include their data for such a high Reynolds number in the comparisons carried out in the present work.

4.2 Comparison of the theory against experimental data

Comparison of the theory with experimental data for the velocity U_b of the bubbles in a bubbly flow as a function of the void fraction is presented in figure 3. One data set corresponds to the experiments conducted by Zenit *et al.*[2] to study a monodispersed suspension of bubbles moving in a vertical channel satisfying the dual limit of large Reynolds number and small Weber number. The mixture is produced by bubbling gas at a constant volumetric flow rate through a stagnant liquid. They used a dilute aqueous electrolyte solution with gas nitrogen. A monodispersed suspension is obtained with the addition of a salt to the liquid, that helps preventing bubble coalescence. The mean equivalent bubble diameter of the suspension increases from 1.364 mm to 1.696 mm for gas volume fraction in the interval $0 \lesssim \alpha \leqslant 0.20$. The aspect ratio decreases in this interval from 1.3 to 1.1 and the Reynolds and Weber numbers decrease with the void fraction from $Re_\mathrm{b} = 380$ and $We_\mathrm{b} = 1.5$ for $\alpha \approx 0$ to $Re_\mathrm{b} = 260$ and $We_\mathrm{b} = 0.5$ for $\alpha = 0.20$. For this data set, Zenit *et al.* gives the fitting $U_\mathrm{b} = U_0(1-\alpha)^n$, with $U_0 = 0.269$ m s^{-1} and $n = 2.796$. They report that $U_0 < U_\infty = 0.320$ m s^{-1}, measured from the rising of a single bubble in a larger pipe, a value that is just within 1% of the result predicted by the theory for an oblate ellipsoid[67]. This sudden steep decrease in bubble velocity with gas concentration for very dilute suspensions has been attributed by Zenit *et al.* to the effects of bubble-wall collisions. They discuss this issue in depth while including additional experimental evidence, and the interested reader should refer to their work. Another data set is taken from the series of experiments performed by Martinez-Mercado *et al.*[39] with a flux of gas nitrogen bubbling through a variety of stagnant liquids. We choose the set of measurements obtained with a mixture of water-glycerin (15% wt.) because the bubbles were nearly spherical and the Reynolds number was $O(100)$. In the experiments with this liquid, the mean bubble diameter decreases from 1.3 to 1.2 mm with increasing void fraction from 0 to 0.05, whereas the aspect ratio remained constant about 1.05. The measured Reynolds and Weber numbers decrease from $Re_\mathrm{b} = 120$ and $We_\mathrm{b} = 0.60$ to $Re_\mathrm{b} = 70$ and $We_\mathrm{b} = 0.22$ for void fraction increasing in the range $0 \lesssim \alpha \leqslant 0.05$. Again, a rapid decrease in the bubble velocity in the region of a very dilute suspension was observed as the velocity for a single bubble in an infinite medium is 0.287 m s^{-1} computed from the theory for a clean oblate ellipsoidal bubble[67] (note that they reported the value of Re_∞ instead). They speculate that the sudden increase in the drag that slows down the bubbles might be caused by velocity fluctuations arising from bubble-wall collisions.

1 The predictions from the irrotational theories described here are compared with the experimental data for the dimensionless velocity U_b/U_∞ in figure 3, where U_∞ takes the values given above for both experimental data sets. In addition, Zenit *et al.* took the model by Spelt and Sangani[32] for the drag coefficient and found an expression for the normalized bubble velocity U_b/U_∞ for vertical bubbly flow through stagnant liquid

$$\frac{U_\mathrm{b}}{U_\infty} = \frac{(1-\alpha)}{1+\frac{3}{20}\alpha A}. \tag{4.7}$$

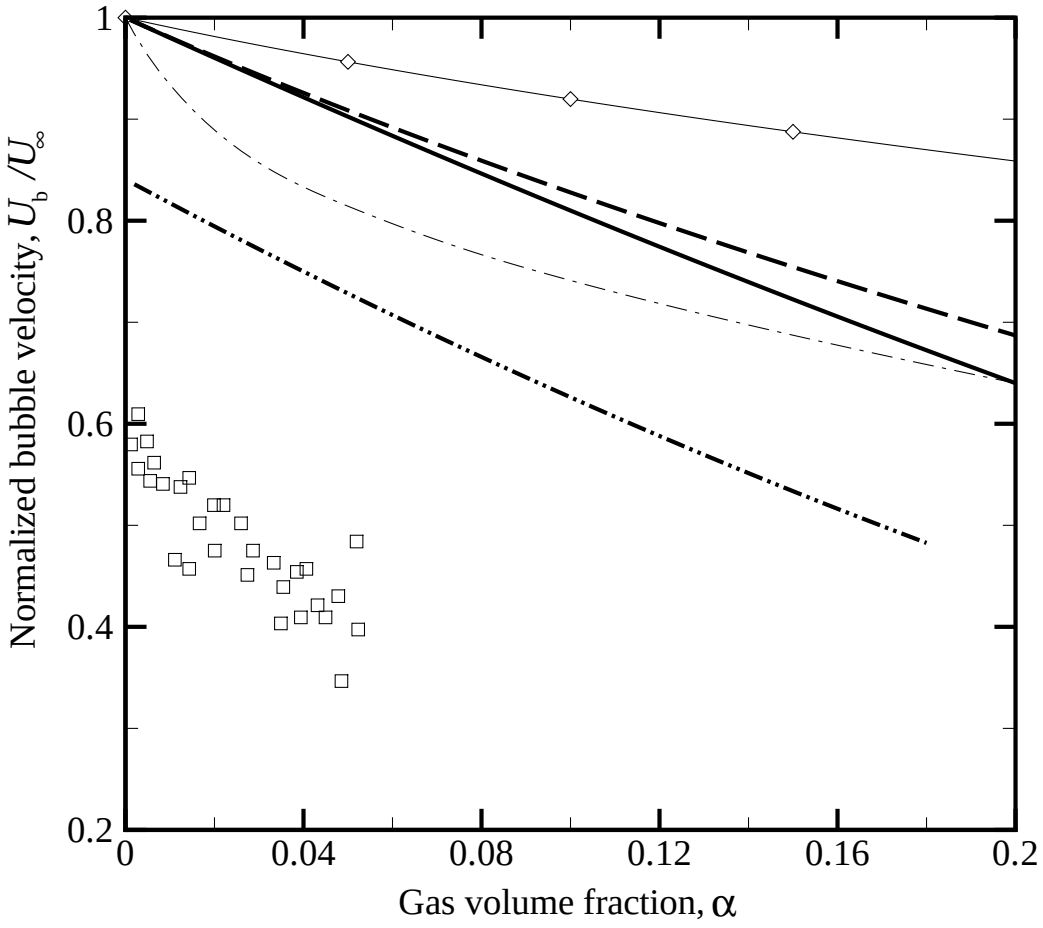

Figure 3: Normalized bubble velocity U_b/U_∞ as a function of the gas volume fraction α for gas bubbling continuously in a stagnant liquid. Two data sets from experiments are included for comparison. Thick dash-dot-dotted line: fitting of data from experiments with nitrogen in aqueous solution by Zenit *et al.*[2]; □: experiments with nitrogen in water-glycerin (15% wt.) by Martinez-Mercado[39]; thick dashed line: DM with zero tangential stress on the outer boundary (4.3.b); thick solid line: DM with irrotational tangential stress on the outer boundary (4.3.c); thin dash-dotted line: model by Spelt and Sangani[32] (4.7); thin solid line with ⋄: Marrucci[51]. DM stands for the dissipation method and VPF stands for viscous potential flow. Predictions are given by $U_\mathrm{b} = U/(1-\alpha)$. For the experiments, U_∞ was determined from Moore's theory[67].

Here the parameter A denotes the inverse of the bubble vertical velocity variance normalized by the square of the mean bubble velocity. A fit for $A = A(\alpha)$ with measurements by Zenit *et al.*[2] is given in Kushch *et al.*[30], $A = (0.02 + 0.5\alpha)^{-1}$. This fitting may be regarded as particular for the set of conditions of the experiments from which it is obtained. Predictions from (4.7) are included in figure 3. Note that A does not approach zero as $\alpha \to 0$; this is explained by the oscillations in the bubble trajectory associated with bubble-wall interactions observed in a single bubble experiment[2]. The drag coefficient formula referred to above was derived by Spelt and Sangani by solving for a viscous potential that adds a first order correction in the dimensionless viscosity to the irrotational flow field. Their expression for the drag coefficient depends upon the void fraction and an additional parameter A, defined above, and is needed in their system of average equations for bubbly flow in the regime of large Reynolds and small Weber numbers. They present comparisons with dynamics simulations, in which satisfactory agreement is demonstrated.

The experiments show that greater concentration of bubbles leads to a hindering of their motion and the models follow this trend. Figure 3 indicates that the theory overpredicts the measurements in the interval of gas volume fraction considered. This trend has been reported by Zenit *et al.*[2] from the comparison of their data with the model by Spelt and Sangani[32]. This discrepancy was attributed to several factors, namely, bubble deformation, departures of the liquid dynamics from irrotational motion due to the presence of surface-active contaminants, and energy dissipation associated with bubble shape oscillations[2]. A similar discrepancy was noted by Kushch *et al.*[30] after comparing their model, derived using an effective-medium theory for oblate spheroidal bubbles, with the data by Zenit *et al.* They suggest that viscous dissipation originated by the container walls might be the cause of such a discrepancy. Figure 3 shows that the model by Spelt and Sangani for U_b/U_∞ presented in Zenit *et al.*, with the fit for A obtained from their experimental data, gives the best approximation to the measurements. Moreover, the difference for all models is the least with the data by Zenit *et al.*, for which the Reynolds number ($380 \geq Re_\mathrm{b} \geq 260$) is about three times that of Martinez-Mercado *et al.* This is consistent with the notion that the formulae considered here is valid for $Re_\mathrm{b} \gg 1$, and thus these models ought to be considered limiting cases as long as the bubbles remain nearly spherical (i.e., $We_\mathrm{b} < 1$).

From the set of viscous irrotational theories analyzed in §§2 and 3, that obtained from the dissipation method with an irrotational tangential stress on the outer boundary gives the smallest discrepancy and also depicts the same slope as the data set by Zenit *et al.* Nevertheless, when the bubbles are modeled as oblate ellipsoids using Moore's[67] model for U_∞, and the variation of the equivalent diameter of the bubbles and aspect ratio with the void fraction is accounted for, the curve of U/U_∞ versus α for the experimental data by Zenit *et al.* becomes rather concave, as presented in their work (not shown here), resembling the curvature of the graph rendered by the model of Spelt and Sangani.

5 Closing remarks

The assumed irrotational dynamics of the incompressible fluid surrounding a spherical bubble of variable radius and bounded externally by a spherical surface, is applied to the computation of the drag acting on the bubble and on the outer surface when a relative translation exists between them. A simpler computation of the drag is given by the integration of the irrotational normal stress, including the viscous part. Another viscous irrotational formulation based upon the mechanical energy balance, namely, the dissipation method, is employed, leading to a different form of the drag. A major aspect of the formulation of the dissipation method presented here is the way the tangential stress boundary condition on the exterior surface enters the analysis. Two choices are considered for this boundary condition, namely, a zero tangential stress and an irrotational tangential stress. In particular, when the bubble volume is held constant, these expressions for the drag are taken as an approximation, in the sense of the classical cell model, of the drag acting on a swarm of identical bubbles. These results are then used to find expressions for the suitably normalized terminal rise velocity of the bubble swarm. These formulae are evaluated by

comparing against other theoretical approaches, numerical simulations of the cell-model and experimental data for bubbly flow.

The results for the drag coefficient obtained by the dissipation approximation in a cell with either a zero tangential stress or an irrotational tangential stress on the exterior surface show fair agreement with results given in the literature from numerical solutions of the steady incompressible Navier-Stokes equations for a free-surface cell model or a zero-vorticity cell model, respectively, for a bubble-swarm Reynolds number Re=100. Similar trend is observed for the bubble swarm terminal rise velocity normalized by the terminal rise velocity of a bubble according to the dissipation method, U/U_∞, for nonzero gas volume fraction, $\alpha \geqslant 0.1$. This bubble swarm rise velocity is found by the equilibration of the viscous drag and bubble weight with the buoyancy force determined by the gas-liquid mixture density. In the infinite dilution limit, the bubble velocity is still larger than the value given by the dissipation method, which should be approached as Re increases. On the other hand, the simpler integration of the normal stress from viscous potential flow gives unsatisfactory predictions. The comparison with the experimental data for bubble velocity in bubbly flow through a stagnant liquid, indicates that the model by Spelt and Sangani, which requires knowledge of the bubble vertical velocity variance, gives the best approximation; it is followed by predictions from the dissipation method with an exterior irrotational-tangential-stress boundary condition.

Acknowledgements

We are indebted to Professor R. Fosdick for his contribution in the preparation of Appendix B. This work was partially supported by grant No. 0302837 from the National Science Foundation. J.C.P. also gratefully acknowledges support from the University of Minnesota Graduate School Dissertation Fellowship. We are thankful to the referees for their constructive criticisms and helpful suggestions that enable us to improve upon an earlier version of the paper.

Appendix A: Force on the outer boundary by the dissipation method

In this analysis we obtain an expression for the force D_2 that the fluid in V exerts on the outer boundary S_2 in the $\mathbf{e}_x$-direction by used of the dissipation method. The analysis involves writing the equations of motion with respect to a noninertial coordinate system. This procedure parallels that of §2.3 for the force D_1 on the bubble interface S_1 when the outer boundary S_2 is a free surface.

The incompressible Navier-Stokes equations relative to the laboratory reference frame are

$$\rho\left(\frac{\partial \mathbf{u}}{\partial t} + \mathbf{u}\cdot\nabla\mathbf{u}\right) = -\nabla p + \mu\nabla^2\mathbf{u}, \tag{A.1}$$

$$\nabla\cdot\mathbf{u} = 0. \tag{A.2}$$

Consider a noninertial reference frame with an origin that moves with velocity $U\mathbf{e}_x$ relative to the laboratory frame and does not rotate. The transformation between coordinate systems is governed by the relations

$$\hat{\mathbf{x}} = \mathbf{x} - \int_0^t U(t')\mathbf{e}_x dt', \qquad \hat{t} = t, \qquad \mathbf{v} = \mathbf{u} - U\mathbf{e}_x. \tag{A.3.a, b, c}$$

The form of the incompressible Navier-Stokes equations is invariant under the transformation (A.3) provided a pseudopressure $\hat{p}$ is defined as[68]

$$\hat{p} \equiv p + \rho\dot{U}\mathbf{e}_x\cdot\hat{\mathbf{x}}, \tag{A.4}$$

so that the governing equations in the noninertial reference frame may be written as

$$\rho\left(\frac{\partial \mathbf{v}}{\partial \hat{t}} + \mathbf{v}\cdot\hat{\nabla}\mathbf{v}\right) = -\hat{\nabla}\hat{p} + \mu\hat{\nabla}^2\mathbf{v}, \tag{A.5}$$

$$\hat{\nabla}\cdot\mathbf{v} = 0. \tag{A.6}$$

With $\hat{\mathbf{T}} \equiv -\hat{p}\mathbf{1} + \mu\left(\hat{\nabla}\mathbf{v} + \hat{\nabla}\mathbf{v}^T\right)$, the right-hand side of (A.5) is $\hat{\nabla}\cdot\hat{\mathbf{T}}$. Moreover, with (A.4),

$$\hat{\mathbf{T}} = \mathbf{T} - \rho\dot{U}\mathbf{e}_x\cdot\hat{\mathbf{x}}. \tag{A.7}$$

Let

$$\hat{D}_2 \equiv -\int_{S_2}\mathbf{n}_2\cdot\hat{\mathbf{T}}\cdot\mathbf{e}_x dA. \tag{A.8}$$

With (2.8) and (A.7), (A.8) yields

$$\hat{D}_2 = D_2 + \int_{S_2}\rho\dot{U}\mathbf{e}_x\cdot\hat{\mathbf{x}}(\mathbf{n}_2\cdot\mathbf{e}_x)dA. \tag{A.9}$$

The fluid motion is subjected to the following boundary conditions:
On S_1,

$$\mathbf{n}_1\cdot\mathbf{v} = \hat{q}_1, \tag{A.10}$$

$$\mathbf{n}_1\cdot\hat{\mathbf{T}}\cdot\mathbf{t}_1^{(\alpha)} = \mathbf{n}_1\cdot\mathbf{T}\cdot\mathbf{t}_1^{(\alpha)} = 0, \qquad \text{for} \quad \mathbf{t}_1^{(\alpha)}\perp\mathbf{n}_1. \tag{A.11}$$

On S_2,

$$\mathbf{n}_2\cdot\mathbf{u} = q_2, \tag{A.12}$$

$$\mathbf{n}_2\cdot\hat{\mathbf{T}}\cdot\mathbf{t}_2^{(\alpha)} = \mathbf{n}_2\cdot\mathbf{T}\cdot\mathbf{t}_2^{(\alpha)} = 0, \qquad \text{for} \quad \mathbf{t}_2^{(\alpha)}\perp\mathbf{n}_2, \tag{A.13}$$

and thus both surfaces are taken as free surfaces. Taking the inner product of (A.5) with $\mathbf{v}$ and invoking (A.6), leads to the mechanical energy equation for the motion relative to the noninertial reference frame. That is, in integral form,

$$\frac{d\hat{E}}{d\hat{t}} = -\int_{S_1}\mathbf{n}_1\cdot\hat{\mathbf{T}}\cdot\mathbf{v}\ dA + \int_{S_2}\mathbf{n}_2\cdot\hat{\mathbf{T}}\cdot\mathbf{v}\ dA - \int_V 2\mu\hat{\mathbf{D}}[\mathbf{v}]:\hat{\mathbf{D}}[\mathbf{v}]\ d\mathcal{V}, \tag{A.14}$$

where,

$$\frac{d\hat{E}}{d\hat{t}} = \frac{d}{d\hat{t}}\int_V \rho\frac{|\mathbf{v}|^2}{2}\,d\mathcal{V} = \int_V \mathbf{v}\cdot\rho\left(\frac{\partial\mathbf{v}}{\partial\hat{t}} + \mathbf{v}\cdot\hat{\nabla}\mathbf{v}\right)d\mathcal{V}, \tag{A.15}$$

and $\hat{\mathbf{D}}[\mathbf{v}] = \frac{1}{2}\left(\hat{\nabla}\mathbf{v} + \hat{\nabla}\mathbf{v}^T\right)$.

With (A.3.c) and (A.8), (A.11) and (A.13), (A.14) may be written as

$$\hat{D}_2 = \frac{1}{U}\left(\frac{d\hat{E}}{d\hat{t}} + \int_V 2\mu\hat{\mathbf{D}}[\mathbf{v}]:\hat{\mathbf{D}}[\mathbf{v}]\ d\mathcal{V} - \hat{W}\right), \tag{A.16}$$

where,

$$\hat{W} = -\int_{S_1}\mathbf{n}_1\cdot\hat{\mathbf{T}}\cdot\mathbf{n}_1\hat{q}_1\ dA + \int_{S_2}\mathbf{n}_2\cdot\hat{\mathbf{T}}\cdot\mathbf{n}_2 q_2\ dA. \tag{A.17}$$

Now, the integrals in the left-hand side of (A.16) are evaluated in potential flow, $\mathbf{v} = \hat{\nabla}\hat{\phi}$. Momentum balance (A.5) reduces to the Bernoulli equation for potential flow, i.e.

$$\frac{\hat{p}}{\rho} + \frac{\partial \hat{\phi}}{\partial \hat{t}} + \frac{|\mathbf{v}|^2}{2} = B(\hat{t}). \tag{A.18}$$

Then, (A.15) yields

$$\frac{d\hat{E}}{d\hat{t}} = -\int_{S_1} (-\hat{p})\hat{q}_1 dS + \int_{S_2} (-\hat{p}) q_2 dS - U \int_{S_2} (-\hat{p}) \mathbf{n}_2 \cdot \mathbf{e}_x dS. \tag{A.19}$$

Denoting $\hat{\mathbf{D}} = \hat{\mathbf{D}}[\mathbf{v} = \nabla\hat{\phi}]$, the dissipation integral in (A.16) becomes

$$\begin{aligned}
\int_V 2\mu \hat{\mathbf{D}} : \hat{\mathbf{D}} d\mathcal{V} &= -\int_{S_1} \mathbf{n}_1 \cdot 2\mu\hat{\mathbf{D}} \cdot \mathbf{v} dA + \int_{S_2} \mathbf{n}_2 \cdot 2\mu\hat{\mathbf{D}} \cdot \mathbf{v} dA \\
&= -\int_{S_1} \mathbf{n}_1 \cdot 2\mu\hat{\mathbf{D}} \cdot \mathbf{n}_1 \hat{q}_1 dA - \int_{S_1} \mathbf{n}_1 \cdot 2\mu\hat{\mathbf{D}} \cdot \mathbf{t}_1^{(\alpha)} (\mathbf{t}_1^{(\alpha)} \cdot \mathbf{v}) dA \\
&- U \int_{S_2} \mathbf{n}_1 \cdot 2\mu\hat{\mathbf{D}} \cdot \mathbf{e}_x dA + \int_{S_2} \mathbf{n}_2 \cdot 2\mu\hat{\mathbf{D}} \cdot \mathbf{n}_2 q_2 dA \\
&+ \int_{S_2} \mathbf{n}_2 \cdot 2\mu\hat{\mathbf{D}} \cdot \mathbf{t}_2^{(\alpha)} (\mathbf{t}_2^{(\alpha)} \cdot \mathbf{u}) dA,
\end{aligned} \tag{A.20}$$

by use of $\mathbf{v} = \mathbf{u} - U\mathbf{e}_x$ and boundary conditions (A.10) and (A.12). Substitution of (A.19) and (A.20) in (A.16), with (A.17) given by potential flow, leads to

$$\begin{aligned}
\hat{D}_2 &= -\int_{S_2} \left(-\hat{p} + \mathbf{n}_2 \cdot 2\mu\hat{\mathbf{D}} \cdot \mathbf{n}_2\right) \mathbf{n}_2 \cdot \mathbf{e}_x dA + \frac{1}{U} \int_{S_2} \mathbf{n}_2 \cdot 2\mu\hat{\mathbf{D}} \cdot \mathbf{t}_2^{(\alpha)} \left(\mathbf{t}_2^{(\alpha)} \cdot \mathbf{v}\right) dA \\
&- \frac{1}{U} \int_{S_1} \mathbf{n}_1 \cdot 2\mu\hat{\mathbf{D}} \cdot \mathbf{t}_1^{(\alpha)} \left(\mathbf{t}_1^{(\alpha)} \cdot \mathbf{v}\right) dA.
\end{aligned} \tag{A.21}$$

Using (A.4) and (A.9), with $\mathbf{D} = \mathbf{D}[\mathbf{u}] = \hat{\mathbf{D}}[\mathbf{v}]$ from the transformation (A.3), expression (A.21) gives rise to (2.34) in §2.3.1.

Finally, expression (2.35) for $D_1 + D_2$ is obtained by used of the self-equilibration of irrotational viscous stresses. This implies,

$$\int_V \nabla \cdot 2\mu\mathbf{D} \cdot \mathbf{e}_x d\mathcal{V} = -\int_{S_1} \mathbf{n}_1 \cdot 2\mu\mathbf{D} \cdot \mathbf{e}_x dA + \int_{S_2} \mathbf{n}_2 \cdot 2\mu\mathbf{D} \cdot \mathbf{e}_x dA = 0, \tag{A.22}$$

which gives rise to the relation,

$$\begin{aligned}
&\int_{S_1} \mathbf{n}_1 \cdot 2\mu\mathbf{D} \cdot \mathbf{n}_1 (\mathbf{n}_1 \cdot \mathbf{e}_x) dA + \int_{S_1} \mathbf{n}_1 \cdot 2\mu\mathbf{D} \cdot \mathbf{t}_1^{(\alpha)} (\mathbf{t}_1^{(\alpha)} \cdot \mathbf{e}_x) dA \\
= &\int_{S_2} \mathbf{n}_2 \cdot 2\mu\mathbf{D} \cdot \mathbf{n}_2 (\mathbf{n}_2 \cdot \mathbf{e}_x) dA + \int_{S_2} \mathbf{n}_2 \cdot 2\mu\mathbf{D} \cdot \mathbf{t}_2^{(\alpha)} (\mathbf{t}_2^{(\alpha)} \cdot \mathbf{e}_x) dA = 0.
\end{aligned} \tag{A.23}$$

The fact that *each* of the surface integrals in (A.22) vanishes is shown in Appendix B.

Appendix B: The net resultant of the viscous stress on a closed surface in potential flow[‡]

Consider a closed surface S bounding a region V of incompressible Newtonian fluid in which the motion is irrotational. The deviatoric stress is given by $\boldsymbol{\tau} = 2\mu\nabla \otimes \nabla\phi$, where ϕ is the velocity potential that

[‡]R. Fosdick and J. C. Padrino, Aerospace Engineering and Mechanics Department, University of Minnesota, Minneapolis, Minnesota 55455, USA.

satisfies Laplace's equation in V, by continuity, and μ is the dynamic viscosity. Then, the divergence of $\boldsymbol{\tau}$ is zero in V. As a consequence, the statement 'the traction vectors $\mathbf{n}\cdot\boldsymbol{\tau}$ have no net resultant on each and every closed surface in the domain V of flow'[69] follows immediately, since

$$\int_D \nabla\cdot\boldsymbol{\tau}\, d\mathcal{V} = \int_\Gamma \mathbf{n}\cdot\boldsymbol{\tau}\, dA = 0, \tag{B.1}$$

by used of the divergence theorem, where D is an arbitrary volume in V with boundary Γ, and $\mathbf{n}$ is the outward normal unit vector to Γ. The surface integral in (B.1) represents the net irrotational viscous stress over Γ.

A proof of the above statement that the surface integral in (B.1) vanishes for every closed surface in the fluid domain is not obvious for a 'periphractic' region. A three-dimensional region is periphractic 'when it is bounded internally by one or more closed surfaces' (Milne-Thomson[70], p. 97). Thus, a periphractic region has one or more holes embedded in it, but no hole runs through the outer boundary, and thus the volume is simply connected.

Consider now a periphractic three-dimensional region bounded externally by a surface S enclosing a fluid volume V and one or more embedded holes. Suppose the fluid motion in V is irrotational. Consider a closed surface Γ immersed in V. This surface may surround a volume totally filled with fluid or there can be one or more holes enclosed by Γ. We wish to show that

$$\int_\Gamma \mathbf{n}\cdot\boldsymbol{\tau}\, dA = \int_\Gamma \mathbf{n}\cdot 2\mu\nabla\otimes\nabla\phi\, dA = 0\,. \tag{B.2}$$

Using Cartesian index notation, since $\tau_{ij} = 2\mu\phi_{,ij}$ and $\phi_{,ii} = 0$, where ',' denotes partial differentiation with respect to the Cartesian coordinates indexed after it, we may write

$$\tau_{ij} = \varepsilon_{ikt}\varepsilon_{jrs}B_{rk,st}\ , \tag{B.3}$$

provided we take

$$B_{rk} \equiv -2\mu\delta_{rk}\phi\ , \tag{B.4}$$

where ε_{ijk} is the permutation symbol and δ_{ij} is the Kronecker delta. This follows by simple reduction of indices, since, with (B.4), (B.3) yields

$$\tau_{ij} = -2\mu\varepsilon_{ikt}\varepsilon_{jrs}\delta_{rk}\phi_{,st} = -2\mu\varepsilon_{ikt}\varepsilon_{jks}\phi_{,st} = -2\mu(\delta_{ts}\delta_{ij} - \delta_{tj}\delta_{is})\phi_{,st} = 2\mu\phi_{,ij}\,. \tag{B.5}$$

The form of (B.3) is known as a 'Beltrami representation' of the stress (see §4 in Fosdick and Royer-Carfagni[71]). Note that τ_{ij} is symmetric provided B_{ij} is also symmetric. Now, with this representation and using Stokes' theorem, we have

$$\int_\Gamma n_i\tau_{ij}\, dA = \int_\Gamma n_i\varepsilon_{ikt}\varepsilon_{jrs}B_{rk,st}\, dA = 0 \tag{B.6}$$

for every closed surface Γ in V. Thus, (B.2) holds and the net viscous irrotational stress on any closed surface Γ in V is zero.

It is also true that, because of the Beltrami representation above, the moment of the irrotational viscous stress on every closed surface Γ in V about any fixed point (say, the origin of the coordinate system) is zero. That is,

$$\int_\Gamma \mathbf{x}\times(\mathbf{n}\cdot\boldsymbol{\tau})\, dA = 0\ , \tag{B.7}$$

or, in Cartesian index notation,

$$\int_\Gamma \varepsilon_{lmj} x_m n_i \tau_{ij} dA = 0\,. \tag{B.8}$$

By applying the divergence theorem, Joseph[72] obtained (B.7) without using representation (B.3) for a region with no embedded holes.

Both balances together say that any closed surface Γ in V is 'self-equilibrated'. Results (B.2) and (B.7) apply, in particular, to the outer and inner boundaries of V.

Appendix C: Velocity potential coefficients

The expression for q_1 in (3.5) may be rewritten in terms of Legendre polynomials as

$$q_1 = \dot{R}_1 + \dot{\epsilon} P_1(z) - \frac{2}{3}\frac{\epsilon\dot{\epsilon}}{R_1}\left(1 - P_2(z)\right) + O(\epsilon^2), \tag{C.1}$$

where $z = \cos\theta$. Using (3.4) for the potential ϕ, expansion (3.10) for coefficients A_l and B_l, and (3.7) for $\mathbf{n}_1$, we can compute

$$\begin{aligned}
\mathbf{n}_1 \cdot \nabla\phi\big|_{S_1} &= -B_0 R_1^{-2} + 2\epsilon B_0 R_1^{-3} P_1(z) + \sum_{l=1}^{\infty}\left[l A_l^{(0)} R_1^{l-1} - (l+1) B_l^{(0)} R_1^{-l-2}\right] P_l(z) \\
&+ \epsilon\sum_{l=1}^{\infty}\left[l A_l^{(1)} R_1^{l-1} - (l+1) B_l^{(1)} R_1^{-l-2}\right] P_l(z) \\
&+ \epsilon\sum_{l=2}^{\infty}\left[(l-1)^2 A_{l-1}^{(0)} R_1^{l-3} + \{(l+1)^2 - 2\} B_{l-1}^{(0)} R_1^{-l-2}\right]\frac{l}{2l-1} P_l(z) \\
&+ \epsilon\sum_{l=0}^{\infty}\left[(l^2-2) A_{l+1}^{(0)} R_1^{l-1} + (l+2)^2 B_{l+1}^{(0)} R_1^{-l-4}\right]\frac{l+1}{2l+3} P_l(z) + O(\epsilon^2).
\end{aligned} \tag{C.2}$$

Then, satisfying (3.5) with (C.1) and (C.2), applying orthogonality of Legendre polynomials and equating terms of alike powers of ϵ, gives rise to this set of relations for the coefficients (3.10):

$$-B_o R_1^{-2} = \dot{R}_1 \tag{C.3}$$

$$A_1^{(0)} - 2B_1^{(0)} R_1^{-3} = \dot{\epsilon} \tag{C.4}$$

$$2B_0 R_1^{-3} + A_1^{(1)} - 2B_1^{(1)} R_1^{-3} + \frac{2}{5}\left(-A_2^{(0)} + 9B_2^{(0)} R_1^{-5}\right) = 0 \tag{C.5}$$

$$2A_2^{(0)} R_1 - 3B_2^{(0)} R_1^{-4} = 0 \tag{C.6}$$

$$2A_2^{(1)} R_1 - 3B_2^{(1)} R_1^{-4} + \frac{2}{3}\left(A_1^{(0)} R_1^{-1} + 7B_1^{(0)} R_1^{-4}\right) + \frac{3}{7}\left(2A_3^{(0)} R_1 + 16B_3^{(0)} R_1^{-6}\right) = \frac{2}{3}\frac{\dot{\epsilon}}{R_1}, \tag{C.7}$$

and, for $l \geqslant 3$,

$$l A_l^{(0)} R_1^{l-1} - (l+1) B_l^{(0)} R_1^{-l-2} = 0 \tag{C.8}$$

$$\begin{aligned}
l A_l^{(1)} R_1^{l-1} - (l+1) B_l^{(1)} R_1^{-l-2} + \left[(l-1)^2 A_{l-1}^{(0)} R_1^{l-3} + \{(l+1)^2 - 2\} B_{l-1}^{(0)} R_1^{-l-2}\right]\frac{l}{2l-1} \\
+ \left[(l^2-2) A_{l+1}^{(0)} R_1^{l-1} + (l+2)^2 B_{l+1}^{(0)} R_1^{-l-4}\right]\frac{l+1}{2l+3} = 0.
\end{aligned} \tag{C.9}$$

Furthermore, we recall (3.8) and (3.9),

$$B_0 = -R_2^2\dot{R}_2 = -R_1^2\dot{R}_1, \tag{C.10}$$

$$A_l l R_2^{l-1} = B_l(l+1)R_2^{-l-2} \quad \text{for} \quad l \geqslant 1, \tag{C.11}$$

respectively. Note that (C.3) is satisfied by (C.10).

From (C.6) and (C.8), by used of (C.11), we obtain $A_l^{(0)} = B_l^{(0)} = 0$ for $l \geqslant 2$. Then, using these results in (C.9), combined with (C.11), yields $A_l^{(1)} = B_l^{(1)} = 0$ for $l \geqslant 3$.

Next, the system (C.4)-(C.7) gives rise to expressions for $A_1^{(0)}$, $B_1^{(0)}$, $A_1^{(1)}$ and $B_1^{(1)}$. This leads to (3.11), and also to $A_2^{(1)}$ and $B_2^{(1)}$ after some algebra. That is, to first order in ϵ,

$$A_2 = -\frac{3\epsilon\dot{\epsilon}R_1^3R_2^3}{2(R_2^3-R_1^3)(R_2^5-R_1^5)}, \qquad B_2 = -\frac{\epsilon\dot{\epsilon}R_1^3R_2^8}{(R_2^3-R_1^3)(R_2^5-R_1^5)}. \tag{C.12}$$

Notice that, although $A_2 = B_2 = 0$ for $\epsilon = 0$, their time derivatives, needed in the unsteady Bernoulli equation, do not vanish, in general, at $\epsilon = 0$. However, it turns out that the $l = 2$ terms do not contribute at all to the forces on S_1 and S_2 in the $\mathbf{e}_x$-direction with $\epsilon = 0$ because of orthogonality of Legendre polynomials.

Literature Cited

(1) Levich, V. G. *Physicochemical Hydrodynamics*; Prentice-Hall, Inc.: Englewood Cliffs, NJ, 1962. (§§80-83).

(2) Zenit, R.; Koch, D. L.; Sangani, A. Measurements of the Average Properties of a Suspension of Bubbles Rising in a Vertical Channel. *J. Fluid Mech.* **2001**, *429*, 307.

(3) Sangani, A. S.; Didwania, A. K. Dynamic Simulations of Flow of Bubbly Liquids at Large Reynolds Numbers. *J. Fluid Mech.* **1993**, *250*, 307.

(4) Kang, S-Y.; Sangani, A.S.; Tsao, H-K.; Koch, D.L. Rheology of dense bubble suspensions. *Phys. Fluids*, **1997**, *9*, 1540.

(5) Sankaranarayanan, K.; Shan, X.; Kevrekidis, I.G.; Sundaresan, S. Analysis of Drag and Virtual Mass Forces in Bubbly Suspensions using an Implicit Formulation of the Lattice Boltzmann Method. *J. Fluid Mech.* **2002**, *452*, 61.

(6) Esmaeeli, A.; Tryggvason, G. A Direct Numerical Simulation Study of the Buoyant Rise of Bubbles at $O(100)$ Reynolds Number. *Phys. Fluids* **2005**, *17*, 093303.

(7) Landau, L. D.; Lifshitz, E. M. *Fluid Mechanics.* Vol. 6 of Course of Theoretical Physics; Pergamon: Oxford, 1959. (§25).

(8) Dryden, H.; Murnaghan, F.; Bateman, H. *Hydrodynamics*; Dover: New York, 1956 (a complete unabridged reprinting of the National Research Council's Bulletin 84, 1931). (Part II, §1.1).

(9) Ackeret, J. Über exakte Lösungen der Stokes-Navier-Gleichungen inkompressibler Flüssigkeiten bei veränderten Grenzbedingungen. *Z. Angew. Math. Phys.* **1952**, *3*, 259.

(10) Levich, V. G. The Motion of Bubbles at High Reynolds Numbers. *Zh. Eksp. Teor. Fiz.* **1949**, *19*, 18.

(11) Joseph, D. D.; Liao, T. Y. Potential Flows of Viscous and Viscoelastic Fluids. *J. Fluid Mech.* **1994**, *265*, 1.

(12) Moore, D. W. The Boundary Layer on a Spherical Gas Bubble. *J. Fluid. Mech.* **1963**, *16*, 161.

(13) Kang, I. S.; Leal, L. G. The Drag Coefficient for a Spherical Bubble in a Uniform Streaming Flow. *Phys. Fluids* **1988**, *31*, 233.

(14) Joseph, D. D.; Wang, J. The Dissipation Approximation and Viscous Potential Flow. *J. Fluid Mech.* **2004**, *505*, 365.

(15) Moore, D. W. The Rise of a Gas Bubble in a Viscous Liquid. *J. Fluid. Mech.* **1959**, *6*, 113.

(16) Tam, P. D. The Unsteady Drag on a Spherical Bubble at Large Reynolds Numbers. *Appl. Sci. Res.* **1982**, *38*, 247.

(17) Miksis, M.; Vanden-Broeck, J.-M.; Keller, J. B. Rising Bubbles. *J. Fluid. Mech.* **1982**, *123*, 31.

(18) Magnaudet, J.; Legendre, D. The Viscous Drag Force on a Spherical Bubble with a Time-Dependent Radius. *Phys. Fluids* **1998**, *10*, 550.

(19) Ohl, C. D.; Tijink, A.; Prosperetti, A. The Added Mass of an Expanding Bubble. *J. Fluid Mech.* **2003**, *482*, 271.

(20) Yang, B.; Prosperetti, A.; Takagi, S. The Transient Rise of a Bubble Subject to Shape or Volume Changes. *Phys. Fluids* **2003**, *15*, 2640.

(21) Takemura, F.; Magnaudet, J. The History Force on a Rapidly Shrinking Bubble Rising at Finite Reynolds Number. **2004**, *Phys. Fluids 16*, 3247.

(22) Léger, D.; Askovic, R. Viscid Contributions to the Hydrodynamic Flows Past a Rising Spherical Gas Bubble with a Time-Dependent Radius. *Int. J. Non-Linear Mech.* **2006**, *41*, 247.

(23) Magnaudet, J.; Eames, I. The Motion of High-Reynolds-Number Bubbles in Inhomogeneous Flows. *Annu. Rev. Fluid Mech.* **2000**, *32*, 659.

(24) Kulkarni, A.; Joshi, J. Bubble Formation and Bubble Rise Velocity in Gas-Liquid Systems: A Review. *Ind. Eng. Chem. Res.* **2005**, *44*, 5873.

(25) Voinov, O. V; Golovin, A. M. Lagrange Equations for a System of Bubbles of Varying Radii in a Liquid of Small Viscosity. *Fluid Dynamics* **1970**, *5*, 458.

(26) Gavrilyuk, S. L.; Teshukov, V. M. Drag Force Acting on a Bubble in a Cloud of Compressible Spherical Bubbles at Large Reynolds Numbers. *European Journal of Mechanics B/Fluids* **2005**, *24*, 468.

(27) Ilinskii, Y.; Hamilton, M. F.; Zabolotskaya, E. A. Bubble Interaction Dynamics in Lagrangian and Hamiltonian Mechanics. *J. Acoustic. Soc. Am.* **2007**, *121*, 786.

(28) Smereka, P. On the Motion of Bubbles in a Periodic Box. *J. Fluid Mech.* **1993**, *254*, 79.

(29) Wang, N.; Smereka, P. Effective Equations for Sound and Void Wave Propagation in Bubbly Fluids. *SIAM J. Appl. Math.* **2003**, *63*, 1849.

(30) Kushch, V.; Sangani, A. S.; Spelt, P. D. M.; Koch, D. Finite-Weber-Number Motion of Bubbles through a Nearly Inviscid Liquid. *J. Fluid Mech.* **2002**, *460*, 241.

(31) Sangani, A. S. A Pairwise Interaction Theory for Determining the Linear Acoustic Properties of Dilute Bubbly Liquids. *J. Fluid Mech.* **1991**, *232*, 221.

(32) Spelt, P. D. M.; Sangani, A.S. Properties and Average Equations for Flows of Bubbly Liquids. *Appl. sci. Res.* **1998**, *58*, 337.

(33) Zhang, D. Z.; Prosperetti, A. Ensemble Phase-Averaged Equations for Bubbly Flows. *Phys. Fluids* **1994**, *6*, 2956.

(34) Esmaeeli, A.; Tryggvason, G. Direct Numerical Simulations of Bubbly Flows. Part I-Low Reynolds Number Arrays *J. Fluid Mech.* **1998**, *377*, 313.

(35) Esmaeeli, A.; Tryggvason, G. Direct Numerical Simulations of Bubbly Flows. Part II-Moderate Reynolds Number Arrays *J. Fluid Mech.* **1999**, *385*, 325.

(36) Bunner, B; Tryggvason, G. Dynamics of Homogeneous Bubbly Flows. Part 1. Rise Velocity and Microstructure of the Bubbles. *J. Fluid Mech.* **2002**, *466*, 17.

(37) Bunner, B; Tryggvason, G. Dynamics of Homogeneous Bubbly Flows. Part 2. Velocity Fluctuations. *J. Fluid Mech.* **2002**, *466*, 53.

(38) Yin, X; Koch, D.; Verberg, R. Lattice-Boltzmann Method for Simulating Spherical Bubbles with no Tangential Stress Boundary Conditions. *Phys. Rev. E* **2006**, *73*, 026301.

(39) Martinez-Mercado, J.; Palacios-Morales, C.A.; Zenit, R. Measurement of Pseudoturbulence Intensity in Monodispersed Bubbly Liquids for $10< Re <500$. *Phys. Fluids* **2007**, *19*, 103302.

(40) Spelt, P. D. M.; Norato, M.A.; Sangani, A.S.; Greenwood, M.S.; Tavlarides, L. Attenuation of Sound in Concentrated Suspensions: Theory and Experiments. *J. Fluid Mech.* **2001**, *430*, 51.

(41) Dodd, T.L.; Hammer, D.A.; Sangani, A.S.; Koch, D.L. Numerical Simulations of the Effect of Hydrodynamic Interactions on Diffusivities of Integral Membrane Proteins. *J. Fluid Mech.* **1995**, *293*, 147.

(42) Sangani, A.S.; Mo, G. Elastic Interactions in Particulate Composites with Perfect as well as Imperfect Interfaces. *J. Mech. Phys. Solids*, **1997**, *45*, 2001.

(43) Koo, S.; Sangani, A.S. Effective-Medium Theories for Predicting Hydrodynamics Transport Properties of Bidisperse Suspensions. *Phys. Fluids*, **2002**, *14*, 3522.

(44) Koo, S.; Sangani, A.S. Mass Transfer Coefficients for Laminar Longitudinal Flow in Hollow-Fibre Contactors. *J. Fluid Mech.* **2003**, *484*, 255.

(45) Happel, J.; Brenner, H. *Low Reynolds Number Hydrodynamics*; Prentice-Hall, Inc.: Englewood Cliffs, NJ, 1965. (§8.4).

(46) Chhabra, R. P. Further Remarks on the Drag of a Swarm of Bubbles. *Int. J. Engng Sci.* **1995**, *33*, 1849.

(47) Cunningham, E. On the Velocity of Steady Fall of Spherical Particles Through Fluid Medium. *Proc. Roy. Soc.* **1910**, *A83*, 357.

(48) Happel, J. Viscous Flow in Multiparticle Systems: Slow Motion of Fluids Relative to Beds of Spherical Particles. *A.I.Ch.E. Journal* **1958**, *4*, 197.

(49) Kuwabara, S. The Forces Experienced by Randomly Distributed Parallel Circular Cylinders or Spheres in a Viscous Flow at Small Reynolds Numbers. *J. Phys. Soc. Japan* **1959**, *14*, 527.

(50) El-Kaissy, M. M.; Homsy, G. M. A Theoretical Study of Pressure Drop and Transport in Packed Beds at Intermediate Reynolds Numbers. *Ind. Eng. Chem. Fundam.* **1973**, *12*, 82.

(51) Marrucci, G. Rising velocity of a Swarm of Spherical Bubbles. *Ind. Engng. Chem. Fundam.* **1965**, *5*, 224.

(52) Kendoush, A. A. Hydrodynamic Model for Bubbles in a Swarm. *Chem. Eng. Sci.* **2001**, *56*, 235.

(53) LeClair, B. P.; Hamielec, A. E. Viscous Flow through Particle Assemblages at Intermediate Reynolds Numbers—A Cell Model for Transport in Bubble Swarms. *Can. J Chem. Engng.* **1971**, *49*, 713.

(54) Manjunath, M.; Tripathi, A.; Chhabra, R. P.; Sundararajan, T. Numerical Simulation of the Drag on a Swarm of Bubbles. *Int. J. Engng. Sci.* **1994**, **32**, 927.

(55) Sherwood, J. D. The Force on a Growing Bubble in Potential Flow. *Int. J. Multiphase Flow* **1999**, *25*, 705.

(56) Joseph, D. D.; Liao, T. Y.; Hu, H. H. Drag and Moment in Viscous Potential Flow. *Eur. J. Mech.* B/*Fluids* **1993**, *12*, 97.

(57) Strauss, W. A. *Partial Differential Equations: An Introduction*; John Wiley & Sons, Inc.: Hoboken, NJ, 1992. (§10.6).

(58) Zuber, N. On the Dispersed Two-Phase Flow in the Laminar Flow Regime. *Chem. Eng. Sci.* **1964**, *19*, 897.

(59) Joseph, D. D.; Funada, T.; Wang, J. *Potential Flow of Viscous and Viscoelastic Fluids*. Cambridge University Press: New York, 2007. (§12.5).

(60) Nicklin, D. J. Two-phase bubble flow. *Chem. Eng. Sci.* **1962**, *17*, 693.

(61) Zuber, N.; Hench, J. Steady State and Transient Void Fraction of Bubbling Systems and their Operating Limits, Part 1: Steady State Operation. General Electric Company, General Engineering Laboratory. Report No. 62GL100, **1962**.

(62) Richardson, J. F.; Zaki, W. N. Sedimentation and Fluidisation: Part I. *Trans. Instn. Chem. Engrs.* **1954**, *32*, 35.

(63) Poletto, M.; Joseph, D. D. Effective Density and Viscosity of a Suspension. *J. Rheol.* **1995**, *39*, 323.

(64) Ishii, M.; Zuber, N. Drag Coefficient and Relative Velocity in Bubbly, Droplet or Particulate Flows. *AIChE Journal* **1979**, *25*, 843.

(65) White, F. M. *Viscous Fluid Flow*; McGraw-Hill, Inc.: New York, 1974. (§3.10).

(66) Jaiswal, A. K.; Sundararajan, T.; Chhabra, R. P. Simulation of Non-Newtonian Fluid Flow through Fixed and Fluidized Beds of Spherical Particles. *Numer. Heat Transfer, Part A* **1992**, *21*, 275.

(67) Moore, D. W. The Velocity of Rise of Distorted Gas Bubbles in a Liquid of Small Viscosity. *J. Fluid Mech.* **1965**, *23*, 749.

(68) Panton, R. L. *Incompressible Flow*; third ed., J. Wiley: Hoboken, NJ, 2005. (§10.7).

(69) Joseph, D. D. Helmholtz Decomposition Coupling Rotational to Irrotational Flow of a Viscous Fluid. *Proc. Nat. Acad. Sci. U.S.A.* **2006**, *103*, 14272.

(70) Milne-Thomson, L. M. *Theoretical Hydrodynamics*; fifth ed., Macmillan & Co. Ltd: London, 1968 (unabridge republication by Dover, New York, 1996). (§3.75).

(71) Fosdick, R.; Royer-Carfagni, G. A Stokes Theorem for Second Order Tensor Fields and its Implications in Continuum Mechanics. *Int. J. Non-Linear Mech.* **2005**, *40*, 381.

(72) Joseph, D. D. The Role of Potential Flow in the Theory of the Navier-Stokes Equations. *Phys. Fluids* **2008**, *submitted*.

List of Figure Captions

Figure 1: Sketch of a spherical bubble B centered at O' sharing interface S_1 with the incompressible fluid occupying volume V bounded externally by the spherical surface S_2 centered at O. The motion of the bubble B is such that O' moves along the fixed direction $\mathbf{e}_x$ with speed U, and its radius can change with time. The line containing the path of O' also contains O, which is fixed with respect to the laboratory frame. This line is therefore the axis of symmetry of the problem. The separation between O and O' is considered to be small. Because of the incompressibility of the fluid in V, changes in the radius of S_2 occur in accordance with changes in the radius of B. Symbol $\mathbf{n}_1$ denotes the inward unit vector to V on S_1 and $\mathbf{n}_2$ denotes the outward unit vector to V on S_2. Unit vectors $\mathbf{t}_1$ and $\mathbf{t}_2$ are orthogonal to $\mathbf{n}_1$ and $\mathbf{n}_2$, respectively.

Figure 2: (a) Drag coefficient C_{D} as a function of the void fraction α. (b) Normalized bubble swarm rise velocity U/U_∞ as a function of the gas volume fraction α. The graphs for C_{D} vs. α are determined with Re=100, except where indicated. The curves of U/U_∞ vs. α are valid for $Re \gg 1$ but do not explicitly depend on Re. Thin solid line: VPF (4.2.a) and (4.3.a); thick dashed line: DM with zero tangential stress on the outer boundary (4.2.b) and (4.3.b); thick solid line: DM with irrotational tangential stress on the outer boundary (4.2.c) and (4.3.c); thin solid line with $\diamond$: Marrucci[51]; $\blacktriangle$ and $\triangle$: numerical simulations with free-surface cell model by Chhabra[46] for Re=20 and Re=100, respectively, where (4.6) is used for the normalized velocity; $\bullet$ and $\circ$: numerical simulations with zero-vorticity cell model by Chhabra for Re=20 and Re=100, respectively. DM stands for the dissipation method and VPF stands for viscous potential flow. The symbols for $\alpha = 0$ correspond to the numerical results by Manjunath *et al.*[54] using a free-surface cell model. U_∞ denotes the single bubble rise velocity from the dissipation method.

Figure 3: Normalized bubble velocity U_{b}/U_∞ as a function of the gas volume fraction α for gas bubbling continuously in a stagnant liquid. Two data sets from experiments are included for comparison. Thick dash-dot-dotted line: fitting of data from experiments with nitrogen in aqueous solution by Zenit *et al.*[2]; $\square$: experiments with nitrogen in water-glycerin (15% wt.) by Martinez-Mercado[39]; thick dashed line: DM with zero tangential stress on the outer boundary (4.3.b); thick solid line: DM with irrotational tangential stress on the outer boundary (4.3.c); thin dash-dotted line: model by Spelt and Sangani[32] (4.7); thin solid line with $\diamond$: Marrucci[51]. DM stands for the dissipation method and VPF stands for viscous potential flow. Predictions are given by $U_{\mathrm{b}} = U/(1-\alpha)$. For the experiments, U_∞ was determined from Moore's theory[67].